An-Najah National University

Faculty of Graduate studies

Photocatalytic Degradation of Aqueous Methylene Blue and Imidacloprid by Ca Alginate-Supported ZnO Nanoparticles

By

Ahlam Hussein Shafiq Zyuod

Supervisors

Prof. Hikmat Hilal

Dr. Ahed Zyoud

This Thesis Submitted in Partial Fulfillment of the Requirements for the Degree of Master of Chemistry, Faculty of Graduate Studies, at An-Najah National University, Nablus - Palestine.

2021

Photocatalytic Degradation of Aqueous Methylene Blue and Imidacloprid by Ca Alginate-Supported ZnO Nanoparticles

By

Ahlam Hussein Shafiq Zyuod

This Thesis was Successfully Defended on 4/ 2/ 2021 and approved by:

Defense Committee Members	Signature
1. Prof. Hikmat Hilal / Supervisor	
2. Dr. Ahed Zyoud / Co- Supervisor	
3. Dr. Wadee Sultan / External Examiner	
4. Dr. Derar Al-Smadi / Internal Examiner	

Dedication

To myself that endured difficulties until she arrived.

To my first love: father and mother.

To my dear husband Ayoub for his continuous support for me.

To my children who bear my absence

To my sister Saeda, without whom I would not have taken this step

To my dear brother Saed

To my two family.... To them I send all my appreciation and respect.

Acknowledgments

Praise be to Allah, who led me until the end of all my work.

I would like to express my appreciation and thanks to my supervisors, Professor Dr. Hikmat Hilal and Dr. Ahed Zyoud, who with their expertise and experience, have always helped me. I also want to thank Mr. Nafez Dweikat for encouraging my laboratory work and for helping me with my studies.

I would also like to thank both the Palestinian Water Authority and the Middle East Desalination Research Center (MEDRC) for their financial support while I am preparing for my master's degree. Thanks to the University of Science and Technology of the United Arab Emirates for kindly performing XRD characterization and SEM stimulation measurements.

Moreover, I would like to thank my father, mum and second mum (my husband's mother), my sisters, brothers, and friends especially Doaa Sidr, Gadeer Sabana, Majd, and Heba nassar, who have been at my side throughout this search, and I wish I made them proud of my hard work.

الإقرار

انا الموقعة ادناه، مقدمة الرسالة التي تحمل العنوان:

Photocatalytic Degradation of Aqueous Methylene Blue and Imidacloprid by Ca Alginate-Supported ZnO Nanoparticles

أقر بأن ما اشتملت عليه هذه الرسالة إنما هو نتاج جهدي الخاص، باستثناء ما تمت الاشارة اليه حيثما ورد، وأن هذه الرسالة ككل أو جزء منها لم يقدم من قبل لنيل أي درجة أو بحث علمي أو بحثي لدى أي مؤسسة تعليمية او بحثية أخرى.

Declaration

The work provided in this thesis, unless otherwise referenced is my own research work and has not been submitted elsewhere for any other degree or qualification.

Student's Name: **اسم الطالب:** أحلام حسين حفيظ زيود

Signature: **التوقيع:**

Date: **التاريخ:** ٤/٤/٢٠٢١م

List of Contents

No	Content	Page
	Dedication	Iii
	Acknowledgments	Iv
	Declaration	V
	List of Tables	Viii
	List of Figures	Ix
	List of Abbreviations	Xi
	Abstract	Xii
	Chapter One: Introduction	1
1.1	Overview	1
1.2	Advanced oxidation processes (AOPs)	2
1.3	Semiconductor	2
1.4	Zinc Oxide	4
1.5	Alginate	5
1.6	Methylene blue	7
1.7	Imidacloprid	9
1.8	Objectives	11
1.9	Novelty of this work	11
	Chapter Two: Methods and Materials	12
2.1	Chemicals	12
2.2	Materials	12
2.2.1	UV-Visible spectrophotometer	12
2.2.2	Lux metre	12
2.2.3	Centrifuge	13
2.2.4	pH meter	13
2.3	Solutions preparation	13
2.4	Catalysts preparation	14
2.5	Catalyst characterization	15
2.5.1	XRD	15
2.5.2	SEM	15
2.5.3	FT-IR spectrum characterization	15
2.5.4	Catalyst composition determination	15
2.5.5	Thermogravimetric analysis (TGA)	16
2.6	Point of zero charge (Pzc)	16
2.7	Calibration curve for MB	16
2.8	Adsorption study	17
2.8.1	Effect of contact time on adsorption	18
2.8.2	Effect of pH on adsorption	19
2.8.3	Effect of contaminants solution concentration on adsorption	19

2.9	Photocatalytic experiments	19
2.9.1	Effect of MB concentration	20
2.9.2	Effect of catalyst amount on MB degradation	20
2.9.3	Effect of the irradiation time on MB degradation	21
2.9.4	Effect of pH on MB degradation	21
2.9.5	Effect of pH on IM degradation	21
2.9.6	Effect of time of irradiation on IM photodegradation	22
2.10	HPLC analysis	22
2.11	Catalyst recovery and reuse	22
	Chapter Three: Results and Discussion	23
3.1	Catalyst Characterization	23
3.1.1	XRD Characterization	23
3.1.2	Scanning Electron Microscopy (SEM)	26
3.1.3	Energy Dispersive X-ray (EDX) Spectroscopy	28
3.1.4	Fourier-transform infrared spectroscopy (FT-IR) characterization	30
3.1.5	Thermal Studies	33
3.2	Point of zero charges (Pzc)	36
3.3	Adsorption study	39
3.3.1	MB adsorption onto Ca-Alginate	39
3.3.2	MB adsorption onto ZnO@Ca-Alginate (the composite)	41
3.4	Photodegradation of MB	45
3.4.1	Effect of pH on MB photodegradation	46
3.4.2	Effect of MB concentration on photodegradation	48
3.4.3	Effect of catalyst loading on MB photodegradation	48
3.5	Comparison between commercial ZnO and ZnO@Ca-Alginate in photodegradation of MB	49
3.6	IM adsorption onto ZnO@Ca-Alginate	50
3.7	IM photodegradation study	51
3.7.1	Effect of pH on IM photodegradation using ZnO@Ca-Alginate	51
3.8	Confirmation of contaminant mineralization	53
3.8.1	HPLC for MB	53
3.8.2	HPLC analysis of the photodegraded IM solution	56
3.9	Catalyst reuse	58
3.10	Conclusions	59
3.11	Recommendations for future work	60
	References	62
	الملخص	ب

List of Tables

No.	Tittle	Page
Table 1	physical characteristics and molecular structure of MB.[34]	7
Table 2	Particle sizes for ZnO, Ca-Alginate and ZnO@Ca-Alginate.	26
Table 3	EDX weight of ZnO@Ca-Alginate nano composite using three spectrums focused three distinct areas.	29
Table 4	comparison between Ca-Alginate and Na-Alginate IR spectrum bands.	31
Table 5	Thermal decomposition results of Ca-Alginate and the composite.	35
Table 6	%adsorption and amount of adsorbed of MB (40 mL, 40 ppm) on 0.10 g Ca-Alginate after 60 minutes at 30°C ± 5°C, at different pH values.	40
Table 7	Values of %adsorption and amount of adsorbed MB. Measurements were made using MB (40 mL, 40 ppm), 0.10 g ZnO@Ca-Alginate after 60 minutes at 30°C ± 5°C with different pH values.	43
Table 8	Effect of MB concentration on %adsorption and the quantity of removal (qt). Measurements were made using MB (40 mL of 20 and 40 ppm), 0.10 g ZnO@Ca-Alginate after 60 minutes, at 30°C ± 5°C, pH~7.7.	45
Table 9	Effect of pH on values of T.N., T.F. and % degradation. Measurements were made after 30 and 60 min, under direct simulated light using solution of MB (40 ml, 40 ppm) with 0.10 g composite (0.075 g ZnO).	47
Table 10	Effect of MB concentration on values of overall rate, turnover number, turnover frequency and % degradation. Measurement were made after 60 min, using 0.10 g ZnO@Ca-Alginate under solar simulated light, pH =7.7, temperature = 30°C ± 5, volume of.	48
Table 11	Effect of catalyst loading on values of T.N., T.F., and %Degradation for MB. Measurements were made after 60 minutes using 0.10 g ZnO@Ca-Alginate under solar simulated light, pH ~7.7, temperature=30°C ±5, contaminants (40 mL, 40 ppm).	49
Table 12	Concentrations of inorganic ion that resulted from photodegradation of MB. Measurement were made using MB solution (40 mL, 40 ppm) mixed with 0.1 g at two photodegradation times periods.	55
Table 13	Values of Deg.% of MB using recovered ZnO@Ca-Alginate catalyst.	59

List of Figures

No.	Tittle	Page
Figure 1	Mechanisms of charged carrier generation in a semiconductor.	3
Figure 2	Semiconductor photocatalyst in photodegradation reactions [18].	4
Figure 3	The repeating units structure of sodium alginate and the formation of the "egg-box" model by Ca^{2+} cation.[32].	6
Figure 4	Resonance structural formulas for Methylen Blue.	7
Figure 5	Photocatalytic degradation pathway of MB.	8
Figure 6	IM major photolysis processes in water [49].	10
Figure 7	calibration curve for MB.	17
Figure 8	XRD diffraction pattern for commercial ZnO NPs.	23
Figure 9	XRD pattern for Ca-Alginate nanoparticles.	24
Figure 10	XRD pattern for (a) ZnO@Ca-Alginate, (b) Ca-Alginate, ZnO@Ca-Alginate and ZnO.	25
Figure 11	Scanning electron micrograph for ZnO NPs.	26
Figure 12	Scanning electron micrograph for Ca-Alginate.	27
Figure 13	Scanning electron micrograph for ZnO@Ca-Alginate.	27
Figure 14	Scanning electron micrograph for :(A) commercial ZnO, (B) ZnO nanoparticles in the composite.	28
Figure 15	SEM and EDX spectra showing various elements in ZnO@Ca-Alginate.	28
Figure 16	FT-IR spectrum for ZnO.	30
Figure 17	Alginic acid constituentations, where (A) is b-D-mannuronic acid and (B) is a-L-guluronic acid.	30
Figure 18	FT-IR spectrum for (A) Sodium-Alginate, (B) Calcium-Alginate.	31
Figure 19	IR spectrum for: (A) ZnO, (B) Ca-Alginate, (C) ZnO@Ca- Alginate.	32
Figure 20	TGA plot for the thermal behavior of ZnO nanoparticles.	33
Figure 21	TGA/DTG plot for the thermal behavior of Ca-Alginate nanoparticles.	33
Figure 22	TGA & DTG plots of ZnO@Ca-Alginate nanoparticles.	34
Figure 23	TGA plot for the thermal behavior of :ZnO, ZnO@Ca-Alginate and Ca-Alginate nanoparticles.	35
Figure 24	Plot of Δ(pH) vs. initial pH for: (a) Ca-Alginate, (b) ZnO and (c) ZnO@Ca-Alginate. Intercept shows value of Pzc for the solids.	36

Figure 25	MB structure equilibrium (A) at low pH solution [69], (B) at high pH solution (MBV) [67]	38
Figure 26	Plot of Δ(pH) vs. initial pH for for: (A) Ca-Alginate, (B) ZnO@Ca-Alginate (C) ZnO	38
Figure 27	Comparison between the catalyst surface charge and IM surface charge	39
Figure 28	Effect of contact time on MB (40 mL, 40 ppm) adsorption by 0.10 g ZnO@Ca-Alginate; at 30°C ± 5°C and pH = 7.7	42
Figure 29	Possible MB hydrogen interaction with Ca-Alginate at high pH values	44
Figure 30	Effect of pH on MB solution (40 mL, 40 ppm) degradation reaction using 0.10 g of ZnO@Ca-Alginate	46
Figure 31	Comparison between (0.08 g) ZnO and (0.10 g) ZnO@Ca-Alginate in MB degradation. Measurements were made using MB concentration (40 ppm), solution volume=40 mL, pH ~7.7, temperature = 30°C±5	50
Figure 32	Effect of pH on IM (50 mL, 20 ppm) degradation efficiency using 0.10 g of ZnO@Ca-Alginate	51
	Figure 33: Possible IM hydrogen interaction with Ca-Alginate	52
Figure 34	HPLC absorbance chromatogram for sample of 40 mL MB (40 ppm) mixed with 0.10 g catalyst at different times interval	54
Figure 35	HPLC absorbance chromatogram of the peaks area for MB degradation	55
Figure 36	HPLC absorbance chromatogram for a solution of IM (50 mL, 20 ppm) mixed with 0.10 g catalyst for different times (0,90, 320 and 440 minutes) at pH 9 and at temperature 30°C ±5	57
Figure 37	HPLC absorbance chromatogram of the peaks% area for IM degradation	58

List of Abbreviations

MB	Methelene blue
CB	Conduction band
CO_2	Carbon dioxide
E_g	Energy band gap
eV	Electron volt
FT-IR	Fourier transform infrared
h^+	Holes
HOMO	Highest Occupied Molecular Orbital
HPLC	High Performance Liquid Chromatography
LUMO	Lowest Unoccupied Molecular Orbital
OH•	Hydroxyl radical
Ppm	Part per million
Rpm	Round per minute
SEM	Scanning Electron Microscopy
T.F	Turnover frequency
T.N	Turnover number
t_R	Retention time
UV-Vis	Ultraviolet-Visible
VB	Valence band
XRD	X-Ray Diffraction
IM	Imedacloprid
TGA	Thermogravimetric analysis

Photocatalytic Degradation of Aqueous Methylene Blue and Imidacloprid by Ca Alginate-Supported ZnO Nanoparticles

By
Ahlam Hussein Shafiq Zyuod
Supervisors
Prof. Hikmat Hilal
Dr. Ahed Zyoud

Abstract

ZnO nanoparticles have been widely used as semiconductors for treating water from organic pollutants. This work used commercial ZnO and supported nanoparticles for the uptake and photolysis of aqueous organic pollutants. Methylene blue MB (dye) and imidacloprid (an insecticide), which are widely used in the agricultural sector in Palestine, have been studied as organic water pollutants. Na-Alginate was converted to the insoluble Ca-Alginate form and used as a substrate to support ZnO nanoparticles. The resulting ZnO @ Ca-Alginate system characterized in several ways, such as FT-IR, UV-Visible, TGA, SEM, EDX, and XRD. All characterization results confirmed the formation of ZnO in the combined catalyst system, which was used in the study of the photolysis of pollutants under simulated solar light irradiation. High performance HPLC liquid chromatography and UV-vis spectrophotometer were used to identify the remaining contaminants. The results showed that the photolysis of MB (40 ppm) by ZnO @ Ca-Alginate reached 100% loss, while imidacloprid (20 ppm) reached 56% loss during 120 minutes. The pH values and the zero charge point (Pzc) play a major role in the photolysis process. It was also possible to recover and reuse the combined catalyst in novel methyl-protein photocatalysis reactions, and the recovered catalyst retained its efficacy,

with about 98% photolysis of MB. Factors affecting the decomposition process were also studied, such as pollutant concentration, catalyst loading, irradiation time, pH, and radiation density.

Chapter one
Introduction

1.1 Overview

Water pollution is one of the most important challenges being studied recently. it has a direct link to human health. Polluted water usually contains heavy metals and industrial organic contaminants. Different methods and strategies, such as sedimentation, absorption and reverse osmosis were applied to treat the polluted water [1]. Unfortunately, these methods have shortcomings. For example, in adsorption study the contaminant may return to the environment if not treated properly [2]. Drinking water contamination is a serious challenge, as the World Health Organization WHO showed that more than a million people die annually in developing countries due to the lack of clean drinking water [3]. Chlorination is another strategy commonly used for water purification and disinfection. Unfortunately, the chlorine produces carcinogenic compounds such as tri-halo methane [4]. Therefore it is necessary to find new methods for water purification or developing previously known methods to provide clean, safe, low cost, reliable, environmentally-friendly and by-product free water[5-8]

Advanced oxidation methods, that are based on semiconductors nanoparticles, are classified among the best options for water treatment. Composite systems, of semiconductor supported on insoluble substrate

materials with higher adsorption efficiency, can be useful systems to break down pollutants and increase the photo catalyst efficiency [9-13].

1.2 Advanced oxidation processes (AOPs)

Advanced oxidation processes (AOPs) involve chemical reactions which degrade organic contaminant materials by the resulting hydroxyl radical ($OH^{\bullet}$) [14]. Semiconductor metal oxides are commonly used as photocatalysts in these reactions [15]. These processes may work for both industrial organic contaminants (such as Methyle blue) and agricultural pesticides, especially those which do not photodegrade naturally.

1.3. Semiconductor

Semiconductors are materials having conductivity between conductors (usually metals) and insulators [16]. Doping enhances semiconductor conductivity, by introducing impurities into the crystal structure[17] [18]. Two types of doping are known, the n-type and the p-type. The n-type (Negative) doping occurs when a small number of electron-donating atoms (such as phosphorous) are added to a semiconductor (such as silicon). The p-type (Positive) doping occurs if electron acceptor atoms (boron) are added to the semiconductor (silicon), Figure (1) [19].

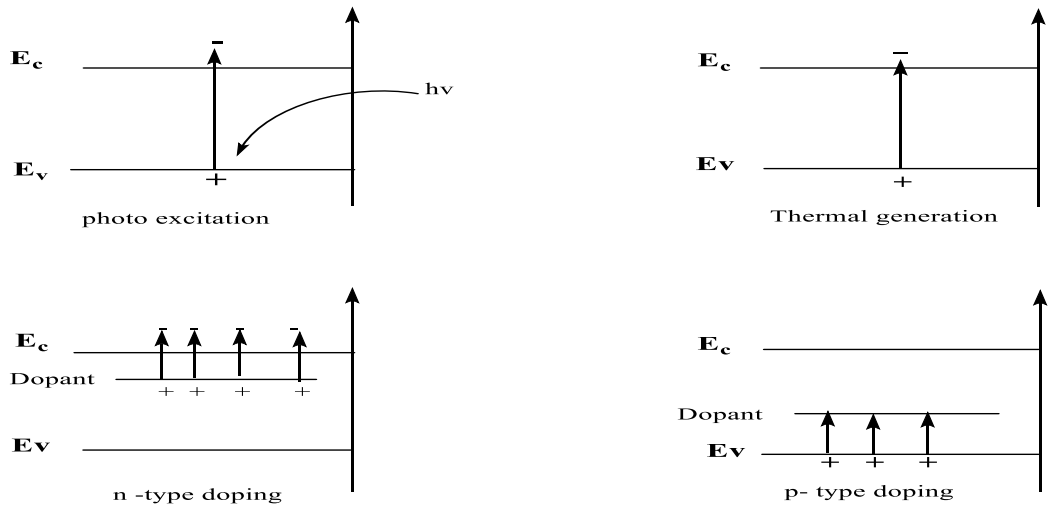

Figure 1: Mechanisms of charged carrier generation in a semiconductor.

In an n-type semiconductor, the Fermi level is closer to the conduction band, while in p-type semiconductors it is closer to the valence band [20]. ZnO is an n-type due to loss of oxygen atoms from the crystal. When oxide ions escape from the crystal as oxygen molecules, they leave their electrons in the crystal behind. ZnO is also a wide bandgap (~3.2 eV) semiconductor [21].

Photodegradation process in water begins when an electron in a semiconductor particle is irradiated by a photon having a suitable energy. The electron (e-) will be excited from the semiconductor valence band (HOMO) to the conduction band (LUMO) leaving a positive hole (h+) behind it [22]. The electric field then separates the electrons and holes in a process called generation process. If electron returns back to the valence band, recombination process occurs [23]. The positive holes at the surface can oxidize nearby molecules (like water and oxygen) [24] to yield a very

reactive hydroxyl radical ($OH^{\cdot}$) that degrades the organic pollutants in water, Figure (2).

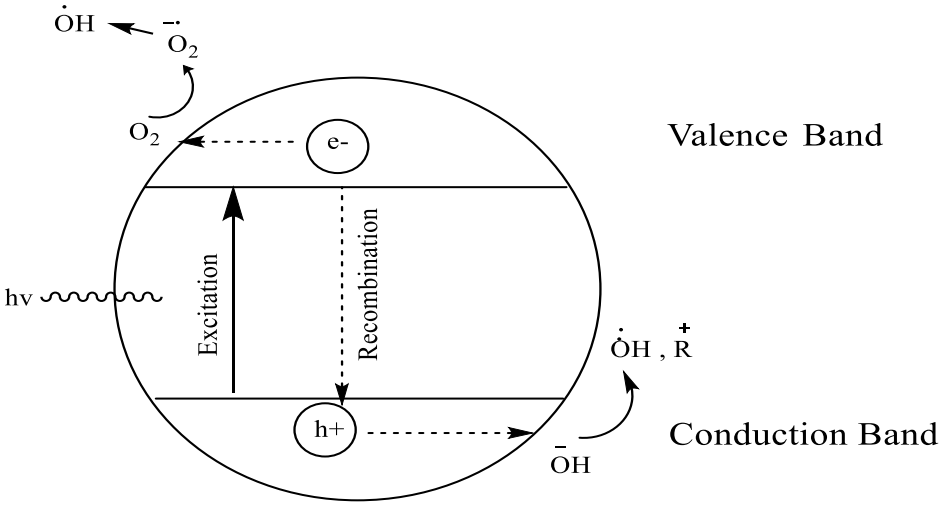

Figure 2: Semiconductor photocatalyst in photodegradation reactions [18].

1.4. Zinc Oxide

Zinc oxide (ZnO) a non-toxic n-type semiconductor with large binding energy (60 MeV), with a wide band gap (~3,2 eV). Both ZnO and TiO_2 are effective photocatalysts [1] but ZnO can absorb UV fraction more than TiO_2 does [25-28]. Therefore, ZnO is advantageous since only about 4% of the solar spectrum falls as UV spectrum [29].

ZnO nanoparticles (ZnO-NPs) have greater efficiency, than larger particles, due to their high relative surface area and their powerful activity against contaminants. Other properties for (ZnO-NPs) are chemical stability, low cost and easy preparations. Therefore, ZnO–NPs are widely studied in water treatment.

Despite the ZnO-NPs advantages, they have drawbacks. The nanoparticles are difficult to separate from the solution. The nanoparticles are also difficult to use in continuous flow reaction systems. ZnO-NPs can also form agglomerate at high loading also [30] which adds to their difficulties. Therefore, it is necessary to support the ZnO-NPs onto insoluble surfaces to make their recovery and re-use easier. Chitosan, cellulose, starch and Alginate have been studied as supporting materials for the ZnO-NPs [31].

1.5. Alginate

"Alginate" is usually the salt of alginic acid. It is natural, non-toxic and abundant at under wide temperature and pH ranges. Adding $CaCl_2$ to the sodium alginate makes it cross-linked and insoluble. The gelatin beads are called calcium alginate [32]. Calcium alginate was chosen in this study to encapsulate ZnO and make a composite with it. The crosslinking properties of calcium cations make it an excellent carrier for many drugs [33]. Calcium alginate nanoparticles were recently synthesized and argued as the novel encapsulation agents for drugs. It has a mean particle size of 400-500 nm [34].

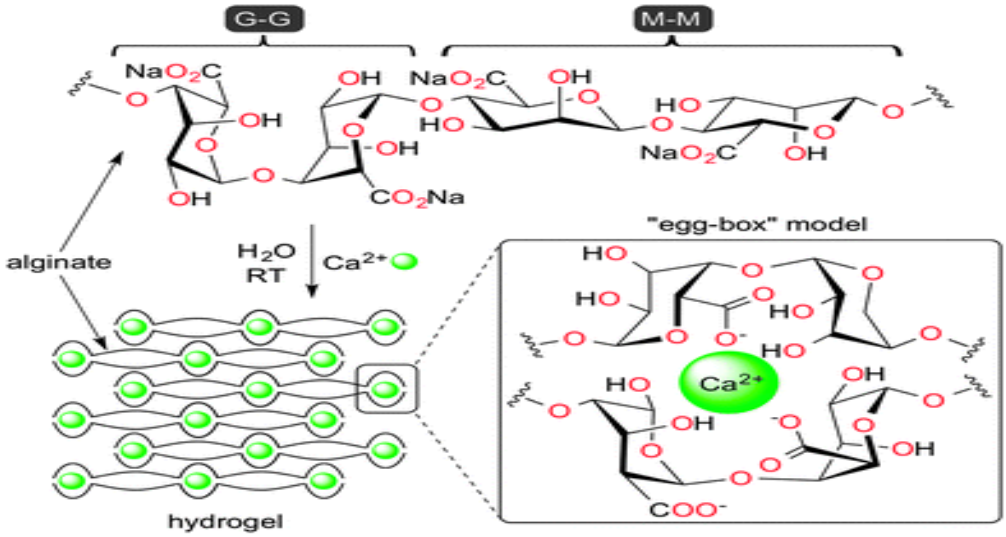

Figure 3: The repeating units structure of sodium alginate and the formation of the "egg-box" model by Ca^{2+} cation.[35]

As shown in Figure (3), Alginate polymers have three types of blocks:

- M-blocks: make an equatorial linkage with mannuronic acid.
- G-blocks: make diaxially-linked with guluronic acid residues leading to more rigidity for the G-blocks.
- MG-blocks: axial–equatorial and equatorial–axial glycosidic bonds connecting the residues [35].

Calcium ions act as a cross linker by forming a hydrogen bond between the functional groups of alginate. It binds to the neighboring G-blocks, causing the "egg-box" model to create ionic inter-chain bridges [36].

1.6 Methylene blue

Methylene blue was firstly prepared in 1876, by Heinrich Caro [37]. It belongs to the thiazine dye group [38]. It has harmful side effects as allergic reactions, headache, vomiting, confusion, shortness of breath and high blood pressure. Pregnant women can also be affected [39] [40]. It also affects the aquatic life by causing a reduction in the dissolved oxygen needed [41].

MB has a green color in its powder, while it's converted to blue in its solution with a pH of 6.5 at 25 °C as shown in Table (1). It has a maximum absorption of light near 670 nm. Methylene blue structural formulas are shown in Figure (4) [42].

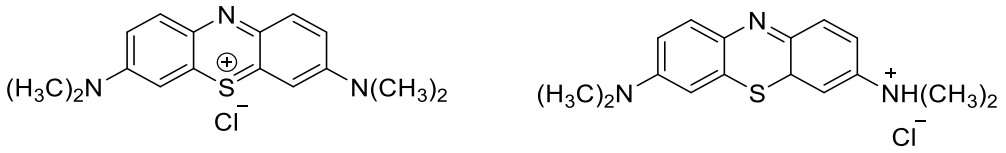

Figure 4: Resonance structural formulas for Methylen Blue.

MB absorption and degradation are affected by various factors such as pH and type of solid surface. MB may also dimerize or aggregate [43].

Table 1: physical characteristics and molecular structure of MB.[34]

Dye name	Methylene Blue
Abbreviation	MB
Class	Thiazine
Max wavelength	663 nm
Colour	Blue
Molecular weight	319.9 g/mol

The degradation route of methylene blue is described in Figure (5). The chloride ions separate as the dye is dissolved. When the hydroxyl radical, coming from semiconductor excitation, attacks the cationic dye, the N-CH_3 bond is broken. The methyl group is oxidized to HCHO or HCOOH. The intermediates are oxidized to single-ring structures, and finally to CO_2 and H_2O [44].

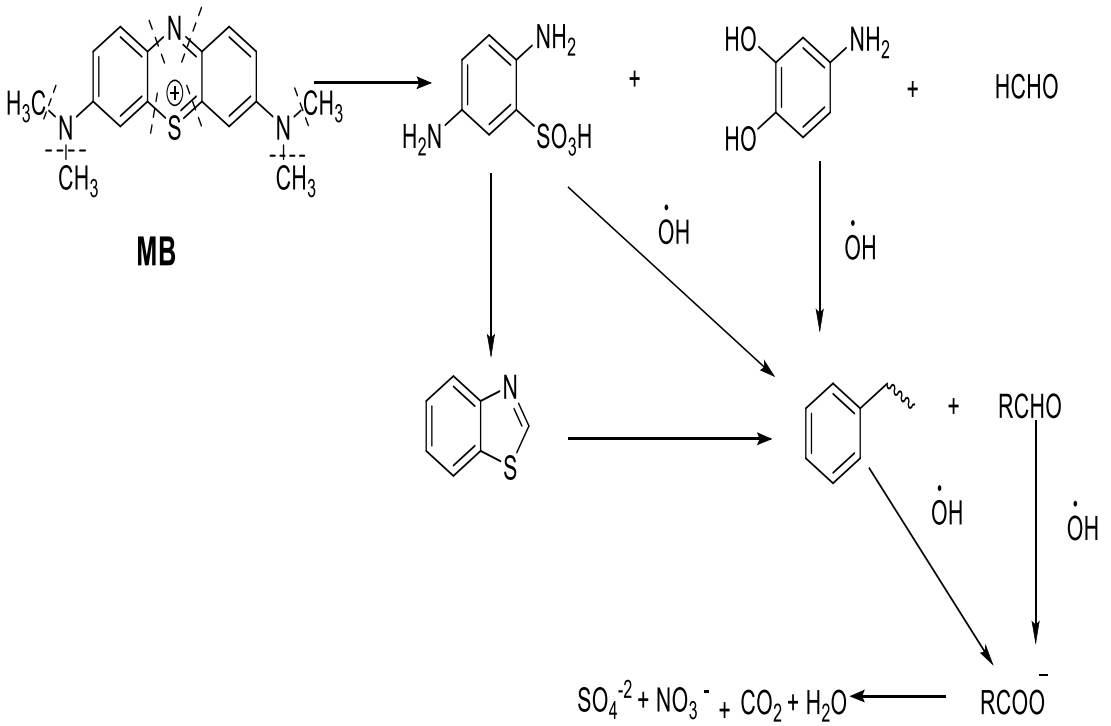

Figure 5: Photocatalytic degradation pathway of MB.

The conversion of organic dyes into minerals as nitrate, ammonium, CO_2 and sulfate ions is important in the photodegradation. The general photocatalysis degradation of the organic pollutant is initiated by the following [45]:

1. $ZnO + hv \longrightarrow e^-_{CB} + h^+_{VB}$

2. Oxygen ion sorption

$(O_2)_{ads} + e^-_{CB} \longrightarrow \bar{O}_2$

3. neutralization of OH^- groups by holes to produce $OH^\cdot$ radicals:

$(H_2O \rightleftharpoons H^+ + OH^-)_{ads} + h_{VB} \longrightarrow H^+ + OH^\cdot$

4. neutralization of O_2 by protons

$\bar{O}_2 + H^+ \longrightarrow HO_2^\cdot$

5. Hydrogen peroxide formation:

$2HO_2^\cdot \longrightarrow H_2O_2 + O_2$

6. Decomposition of H_2O_2 :

$H_2O_2 + e \longrightarrow OH^- + OH^\cdot$

7. Oxidation of organic contaminant by $OH^\cdot$:

$RH + OH^\cdot \longrightarrow \dot{R} + H_2O$

8. Direct oxidation by holes :

$R + h^+_{VB} \longrightarrow R^{\cdot+} \longrightarrow$ Degradation product

1.7 Imidacloprid

Imidacloprid (IM) is an insecticide that was widely used until 1999 [46]. It belongs to a class of chemicals called neonicotinoids. It acts on the central nervous system of insects by blocking the nervous pathway of nicotine which leads to the insect death. This pesticide is considered more toxic to insects than to mammals [47].

Pesticides that contaminate water typically have some characteristics like, high water solubility value (> 30 mg / L), octanol-water coefficient (K_{ow}) < 1, coefficient of organic carbon to water separation (K_{oc}) > 300, the half-life of hydrolysis > 48 days and the half-life of photolysis > 7 days. In addition, at moderate pH values, these pesticides are typically negatively or partially charged.[48]

IM is highly soluble in water (514 ppm) with high potential for leaching into groundwater. IM has a coefficient of organic carbon to water separation (K_{oc}) = (156 – 960). Its capacity for bioaccumulation is low due to its moderate K_{ow} ~ (0.57). IM has a half-life in water more than 31 days which suggest that this insecticide is extremely degradation-resistant [49]. IM has some major photolysis process in water as shown in Figure (6).

IM hydrolysis half-life varies from 33 to 44 days at pH 7 and 25 °C [50]. It is stable in acidic and neutral water, but decomposes readily in basic media [51].

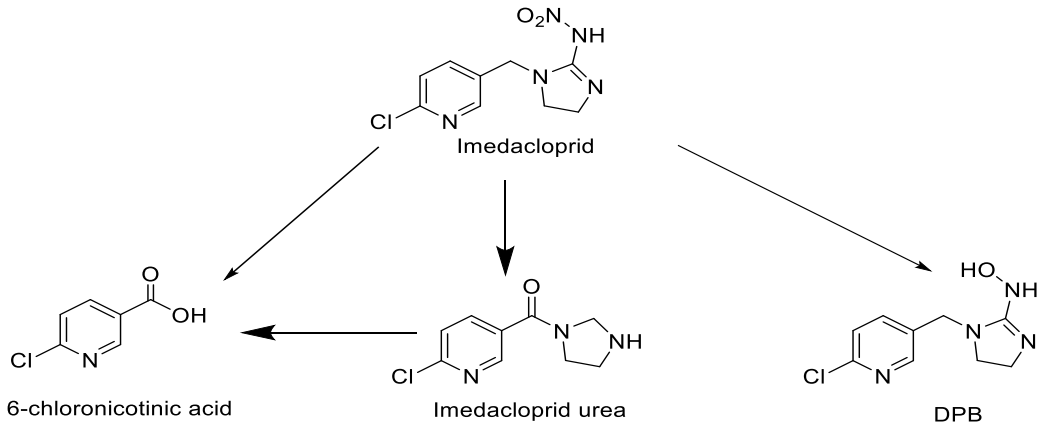

Figure 6: IM major photolysis processes in water [52].

1.8 Objectives

The objectives of this study are to:

1. Prepare calcium Alginate immobilized ZnO beads (ZnO@Ca-alginate beads).
2. Characterize the prepared ZnO@Ca-alginate beads using suitable tests.
3. Determine the photo-catalytic removal efficiency of MB and IM from water using the prepared ZnO@Ca-alginate beads.

1.9 Novelty of this work

Naked Alginate and Alginate supported ZnO and TiO_2 was used in water contaminant removals by adsorption, where this material showed superiority over other materials used in this application [53]. To the best of our knowledge, using ZnO@Ca-alginate composite material in photodegradation process has not been used before. In this work we will prepare ZnO nanoparticles and then we will support the ZnO particles on alginate. The prepared composite materials will then be characterized and used in adsorption and in photodegradation of water organic contaminants.

Chapter Two
Methods and Materials

2.1 Chemicals

Calcium chloride, sodium alginate, Methylene blue MB, and Zinc oxide (ZnO) were purchased from Sigma Aldrich.

Acetic acid, methanol, and acetonitrile solvents for HPLC analysis were purchased from Sigma Aldrich.

Imidacloprid (insecticide solution) was obtained from local markets as a commercial product named Confidor. The Confidor bottle contains 350 g L^{-1} IM as an active ingredient, in addition to some solvents and preservatives, such as 1-methyl-2-pyrrolidone (38%), Dimethyl sulfoxide (39%).

2.2. Equipment

2.2.1 UV-Visible spectrophotometer

A spectrophotometer (Shimadzu UV-1601) was used for Methylene blue (MB) analysis at λ_{663} nm. A calibration curve with different concentrations (10, 20, 30 and 40 ppm) was built up for analysis.

2.2.2 Lux metre

A light intensity meter (Lx-102) was used for the light intensity determination.

2.2.3 Centrifuge

Scientific Ltd model 1020 D.E. centrifuge was used for separation the solid materials from solution.

2.2.4 pH meter

A jenway 3510 pH meter was used for adjusting the solution's pH values.

2.3 Solutions preparation:

0.10 g of MB was dissolved in 100 mL water to prepare a stock solution of 1000 ppm. A different MB concentration solutions were prepared as required.

The stock solution of IM (1000 ppm) was prepared by dissolving 0.286 mL (0.350 g) of IM bottle in 100 mL of distilled water. The stock solution was used to prepare the required concentrations of IM.

Diluted HCl and NaOH solutions were prepared and used for the solutions pH value adjustment.

A Nessler reagent was used for NH_4^+ ion detection after the photodegradation experiments [54].

Cadmium reagent was used for detection of the NO_3^- ions produced by photodegradation experiments [55].

Barium chloride solution was used for detection of the SO_4^{-2} ions produced by the photodegradation experiments [56].

2.4 Catalysts preparation

20 g of zinc oxide were suspended in 200 mL of distilled water to obtain a solution (9.1% w/w). Sodium alginate (2% w/w) was prepared by dissolving 2.0 g in distilled water up to 100 mL solution. The solution was stirred for an hour until the solid was dissolved and give a homogeneous solution. $CaCl_2$ solution (2% w/w) was prepared by dissolving 2.0 g of $CaCl_2$ in distilled water up to 100 mL solution. ZnO suspension was added to the $CaCl_2$ solution with vigorous stirring. Sodium Alginate was added drop-wise to the mixture while stirring. A composite system of ZnO with insoluble Ca-alginate was produced. The produced composite ZnO@Ca-alginate was separated by section filtration. The powder was oven dried at 100 °C for an hour.

To prepare Ca-Alginate, a 100 mL of $CaCl_2$ (2% w/w) solution was drop wised added to a 100 mL of Na-alginate (2% w/w) vigorously stirred solution [57]. The produced beads of insoluble Ca-alginate were filtered, washed with distilled water to eliminate the excess of soluble calcium and chloride ions. The produced solid was then dried at 100°C in the oven for 2 hours.

2.5 Catalyst characterization

2.5.1 XRD

A Philips XRD XPERT PRO diffract meter was used to measure X-ray diffraction patterns. The analysis was performed at UAE University, Al Ain, UAE. XRD patterns were used in determining the size of the particles in the catalyst composite. XRD was also used to confirm the formation of the ZnO@Ca-Alginate nanoparticles.

2.5.2 SEM

A Joel (JSM-6700F) was used to determinate the morphology of the catalyst. The analysis was conducted at UAE University, Al Ain, UAE.

2.5.3 FT-IR spectrum characterization

ZnO@Ca-alginate catalyst was FT-IR analyzed by using Nicolet iS5 Fourier-Transform Infrared Spectroscopy, the FT-IR analyser is connected with Thermo Scientific (iD3 ATR)**.**

2.5.4 Catalyst composition determination

To verify the complex composition and to know the constituent elements and their ratio, energy dispersive (EDX) X-ray spectroscopy was used. The analysis was carried out at the United Arab Emirates University, Al Ain.

2.5.5 Thermogravimetric analysis (TGA)

Deltachem, TGA-1000 was used to understand the structural transformation of ZnO@Ca-Alginate and its stability. The analysis was done under O_2 and N_2 atmosphere respectively with a heating rate of 10 ºC/min. A sample of weight = 36 mg was analyzed from room temperature to 1000 ◦C.

2.6 Point of zero charge (Pzc)

Pzc was calculated using the pH drift method [58]. A 0.01 M NaCl solution had been prepared and boiled to remove CO_2. A diluted NaOH/ HCl solutions were used to adjust the initial pH of the NaCl solution between the range (2-12). 50 mL of the NaCl solution was put in capped glass vial under N_2 gas. The catalyst (0.10 g) was added to each sample and shaken for 8 hours to balance. The final pH of the equilibrated solution was measured. The value of ΔpH (pH_f – pH_i) was plotted against pH_i and the Pzc value for each catalyst were represented by the x- intercept.

2.7 Calibration curve for MB

The MB concentration was determined by using UV-visible spectrophotometry at maximum absorption wavelength of 663 nm. A calibration curve of different MB concentrations (10, 20, 30 and 40 ppm) was built up. The concentration of MB in the analyzed sample was determined based on the calibration curve of MB, Figure (7).

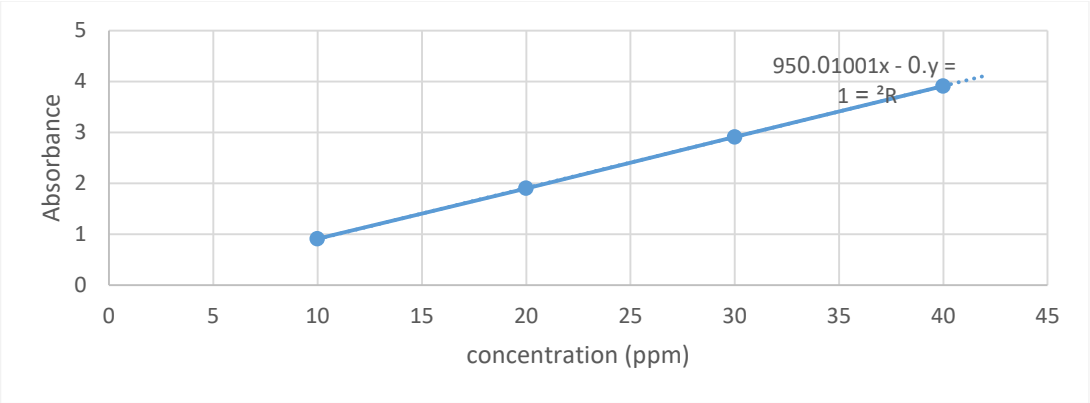

Figure 7: Calibration curve for MB.

2.8 Adsorption study

Batch experiments were performed to study the contaminants adsorption onto the surfaces of Ca-Alginate and ZnO@Ca-Alginate. A 0.10 g of the adsorbent was mixed with a contaminant's solution at appropriate concentrations in each experiment. It was stirring in the dark at 30°C ±5. Aliquots were taken from the solution during specific time periods. The syringed aliquots were centrifuged at 6000 r/min for 6 minutes. The contaminant concentration was analyzed by UV-vis spectrophotometer for MB and by using HPLC for IM.

The following equation was used to determine the amount of adsorption (q_t) by the catalyst at time t:

$$q_t = \frac{(C_0 - C_t)}{m} V \quad \text{----------} \quad (2.1)$$

And the adsorption efficiency (% adsorption) was estimated from the following equation:

$$\% \text{ Adsorption} = \frac{(C_0 - C_t)}{C_0} * 100\% \quad \text{---------- (2.2)}$$

Where q_t is the amount of contaminant per gram of catalyst at any time *t* (mg/g), C_0 is the adsorbate initial concentration (ppm), C_t is the adsorbate concentration at time t, V is the volume of solution (liters), and m is the mass of catalyst in grams [59].

Different parameters such as effect of contact time, effect of pH, and effect of adsorbate concentrations were studied.

2.8.1 Effect of contact time on adsorption.

The effect of contact time on adsorption process was studied. Appropriate concentrations of the contaminant's solution (40 ml, 40 ppm for MB and 50 ml, 20 ppm for IM) were mixed with 0.10 g catalyst each time. The solution then was stirred in the dark at pH ~ (7.7, 9) for MB and IM respectively. liquors were syringed at different time periods (0, 10, 15, 30, 60, 120 and 300 minutes), centrifuged and analyzed as described previously.

2.8.2 Effect of pH on adsorption.

Appropriate concentrations of the contaminant's solution (40 ml, 40 ppm for MB and 50 ml, 20 ppm for IM) were mixed with 0.10 g catalyst each time. Different pH values were adjusted as desired by addition of diluted NaOH/HCl solutions. The solution was stirring in dark for 60 minutes at 30 °C± 5.

2.8.3 Effect of contaminants solution concentration on adsorption.

An initial MB concentration of 20 and 40 ppm was mixed with 0.10 g catalyst. The solution was then stirred at temperature (30 °C± 5) until reaching equilibrium (60 minutes). liquors were syringed, centrifuged and analyzed as described previously. The amount of adsorption at equilibrium, q_e (mg/g), was estimated using equation (2.1).

2.9 Photocatalytic experiments

A 400 mL beaker containing a mixture of the catalyst and contaminants solution at appropriate concentrations were used in each experiment. The reaction beaker was thermostated at about 30 °C to keep the reaction temperature stable during the photodegradation experiments.

A simulated solar light lamb (0.0146 w/cm^2 intensity at the reaction surface) was fixed above the beaker of the reaction. Aliquots were taken from the solution during specific time periods. The syringed aliquots were centrifuged at 6000 r/min for 6 minutes. The concentration of contaminants was analyzed by UV-vis spectrophotometer for MB and by HPLC for IM.

The percentage of photodegradation, values of overall rate, turnover number (T.N) and turnover frequency (T.F) were all measured for needed experiment using the following equations: [60]

$$\text{The turn over number (T.N)} = \frac{\text{Moles of MB (contaminant) reacted}}{\text{Moles of catalyst}} \quad \text{---------} \quad (2.3)$$

$$\text{The turn over frequency (T.F)} = \frac{\text{Turn over number}}{\text{Time (min.)}} \quad \text{--------} \quad (2.4)$$

The photodegradation experiments of MB contaminants were conducted at different parameters like different catalyst amounts, different contaminate concentrations, and different pH values (2-12 pH values) to reach the optimum photodergadation conditions.

2.9.1 Effect of MB concentration

Different MB solutions with different concentrations (10, 20, 30 and 40 ppm) were stirred with 0.10 g of the catalyst in the dark for 30 minutes. After that, the mixture was exposed to the simulated solar light for 1 hour. The MB concentrations were examined at different time periods.

2.9.2. Effect of catalyst amount on MB degradation

A 40 mL of 40 ppm of MB solutions were mixed with different catalyst amounts (0.05, 0.1, 0.2, 0.28 and 0.35 g) and stirred in dark for 30 minutes. The mixture was then exposed to simulated solar light irradiation for 60 minutes. The concentrations of MB were analyzed at different time periods.

2.9.3. Effect of the irradiation time on MB degradation.

A 40 mL of 40 ppm of MB solutions was mixed with 0.10 g of the catalyst. The mixture was exposed to simulated solar light irradiation, after stirring them in dark for 30 minutes, at different time periods (30, 60, 120, 180, 240 and 300 minutes). The concentration of MB was analyzed at each time periods.

2.9.4. Effect of pH on MB degradation.

A solution of MB (40 mL, 40 ppm) was mixed with 0.10 g ZnO@Ca-Alginate. The mixtures were exposed to simulated solar light irradiation at different pH values ranged (2-12) for one hour. The pH values were adjusted by adding drops of either diluted HCL/ NaOH solution.

In case of IM degradation, some parameters as the effect of pH and time of irradiation were selected to study their effect on the catalyst efficiency.

2.9.5 Effect of pH on IM degradation.

Photoegradation tests were carried out under simulated solar light irradiation for 2 hour using IM (50 mL, 20 ppm) solution mixed with 0.10 g of catalyst. The initial pH of the solution was modified to various 4-12 values using diluted NaOH solution. Aliquots were centrifuged and analyzed by HPLC.

2.9.6 Effect of time of irradiation on IM photodegradation.

photodegradation experiments were performed using a solution of **IM** (50 mL, 20 ppm) mixed with 0.10 g of catalyst for various periods of time (30, 60, 120, 180, 240 and 420 minutes) under simulated solar light. Aliquots were taken as explained previously and analyzed by HPLC.

2.10 HPLC analysis

The complete degradation and mineralization and the presence of intermediates in photodegradation of MB and IM were confirmed by using HPLC-DAD Water1525. The separation was achieved by C18 column (5 µm, 4.6×250 mm cartridge). The samples of liquors where syringed at different irradiations periods. It then analyzed by using HPLC.

In case of IM mineralization, the mobile phase involved acetic acid (0.1%) and acetonitrile in a ratio (1:1) with a flow rate of 1.6 ml/min, the detection wave length was at 270 nm. The injection volume was 20µ.

For MB mineralization, the mobile phase involved 0.01% phosphoric acid and acetonitrile in a ratio (2:1) in isocratic elution. The flow rate was 1 mL/min. The detection wave length was at 663 nm. The injection volume was 5 µl.

2.11 Catalyst recovery and reuse

The efficiency of the catalyst under reuse was studied in the case of methylene blue. After the photodegradation process is finished, the catalyst was filtered, washed with distilled water and then dried for reuse.

Chapter Three

Results and Discussion

3.1 Catalyst Characterization

3.1.1 XRD Characterization

3.1.1.1 XRD pattern for ZnO

XRD pattern of ZnO in Figure (8) shows peaks with reflections at 2θ (31.87°, 34.52°, 36.35°, 47.52°, 56.57°, 62.93°, 66.44°, 68.03° and 77.04°). This peaks were corresponded respectively, with reflections of (100), (002), (101), (102), (110), (103), (200), (112), (201) and (202) according to Bragg's planes [61]. XRD pattern reflections of the prepared ZnO are consistence with literatures [10, 11, 61], which confirms ZnO identity.

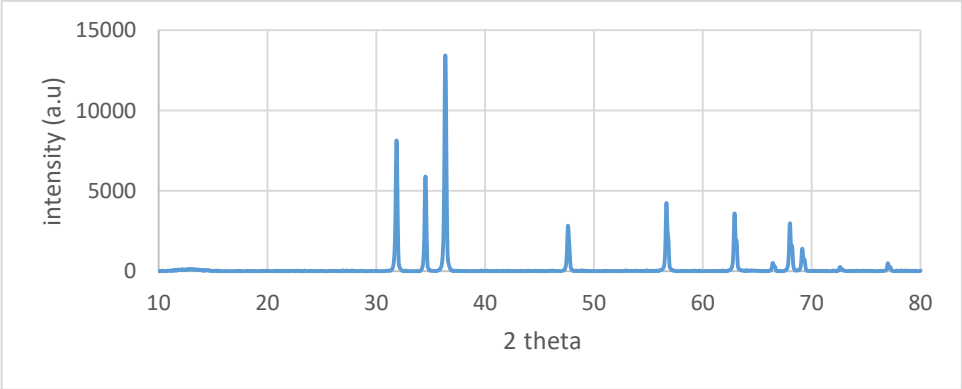

Figure 8: XRD diffraction pattern for commercial ZnO NPs.

ZnO particle size was calculated using Scherrer equation [62]:

$$\boldsymbol{d} = \frac{K\lambda}{B\cos\theta}$$

Where:

- d is the particle diameter (nm),
- K is the shape factor (~ 0.9),
- λ is XRD wavenumber ~ (0.154 nm) and
- β (FWHM): full width at half maximum of the reflection at 2θ (in radian).

Sharp signals for ZnO particles indicate crystallinity structure. The average size of ZnO particles (nm) was estimated using the most intense peaks appeared in the XRD pattern: 31.87°, 34.52° and 36.35°. Closer values were achieved (53.3, 53.9 and 56.81 nm), with an average size value ~ 54.79 nm.

3.1.1.2 XRD pattern for Ca-Alginate.

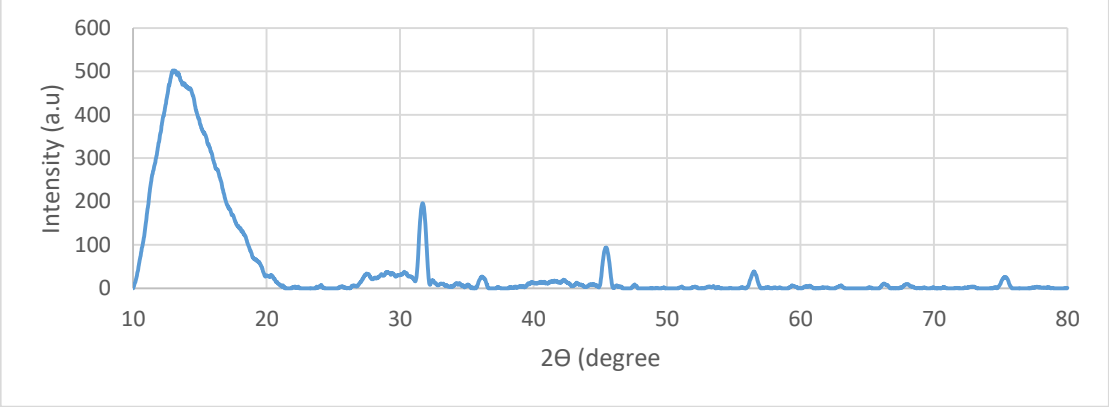

Figure 9: XRD pattern for Ca-Alginate nanoparticles.

As shown in Figure (9), The broadening band which ranged from (10° to 20°) indicates that a smaller particle size was formed. The intense reflections of the Ca-Alginate XRD appeared at 2Ɵ (13.04°, 14.15° and 15.63°). These reflections were used to calculate the size of crystalline by Scherer equation. A very small particle (~ 2.62 nm) was appeared as it was expected.

3.1.1.3 XRD pattern for ZnO@Ca-Alginate.

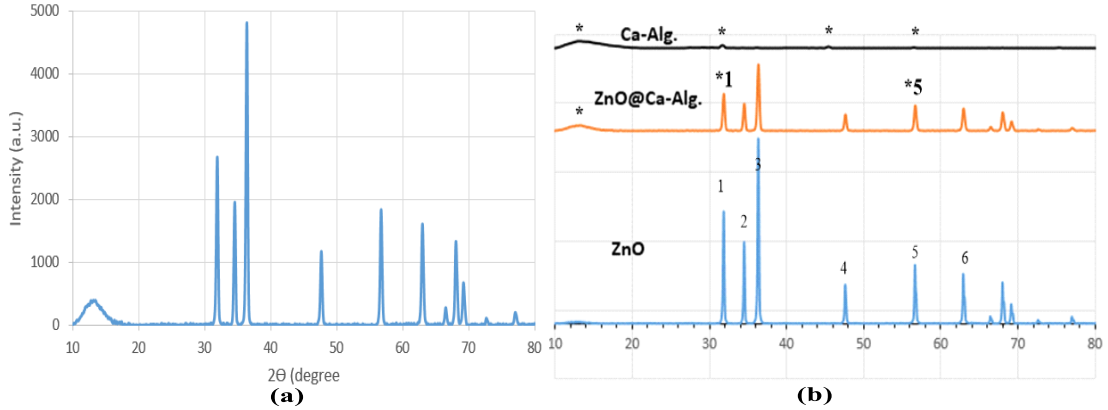

Figure 10: XRD pattern for (a) ZnO@Ca-Alginate, (b) Ca-Alginate, ZnO@Ca-Alginate and ZnO.

The basic diffraction peaks of ZnO (31.87°, 34.53° and 36.36°) and for Ca-Alginate (13.47°and 47.7°) appeared with no shifting in the spectrum as shown in Figure (10). This result confirms that ZnO was supported at the surface of Ca-Alginate successfully. The peaks of supported ZnO show lower intensity and some expansion than the peaks of naked ZnO. It indicates that a decreasing in the particle size of ZnO in the composite was happened. At the other hand, the peaks of the Ca-Alginate particles in the composite appear sharper than the naked one, which

indicates that an increasing in the particle size of Ca-Alginate in the composite was happened as shown in Table (2).

Table 2: Particle sizes for ZnO, Ca-Alginate and ZnO@Ca-Alginate.

Catalyst	ZnO particle size	Ca-Alginate particle size
ZnO	~ 54.79 nm	-
Ca-Alginate	-	~ 2.62 nm
ZnO@Ca-Alginate	30.26 nm	~ 8.75 nm

3.1.2 Scanning Electron Microscopy (SEM)

3.1.2.1 SEM result for ZnO

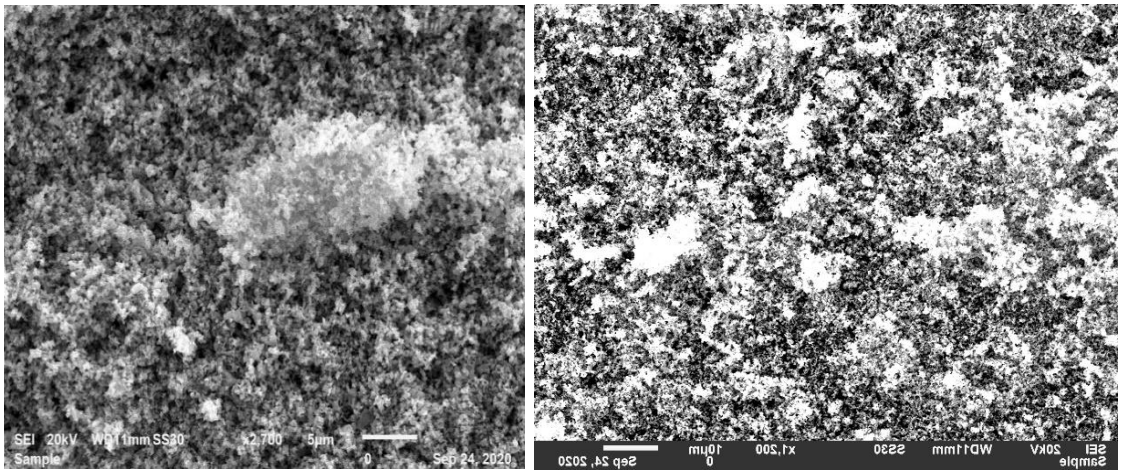

Figure 11: Scanning electron micrograph for ZnO NPs.

Figure (11) shows that Commercial ZnO particles have a uniform structure with some homogenous agglomerates distribution of ~1400 nm diameter.

3.1.2.2 SEM result for Ca-Alginate.

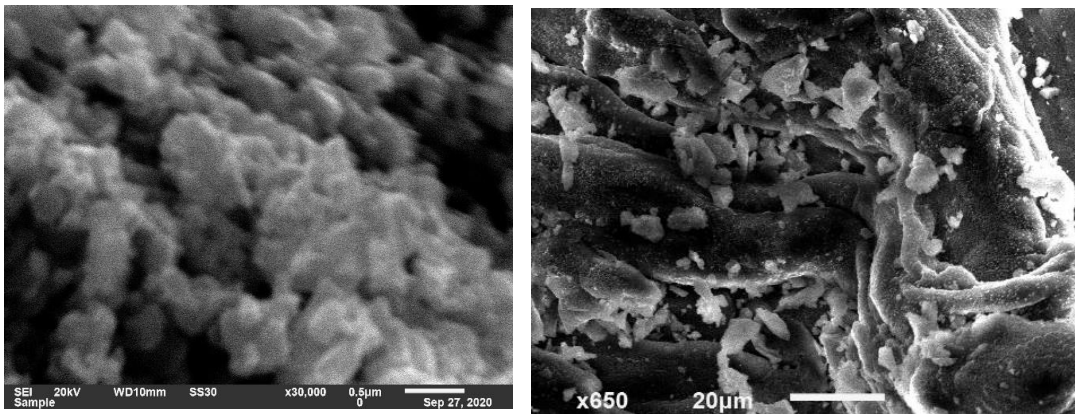

Figure 12: Scanning electron micrograph for Ca-Alginate.

Ca-Alginate morphology can be seen by SEM in Figure (12). It has a rough surface structure with a big grooves and plates. The diameter for Ca-Alginate plates is ~15.2 µm, which make it a good supporting surface. The porous and holes in the Ca-Alginate structure increase its adsorption efficiency.

3.1.2.3 SEM result for ZnO@Ca-Alginate.

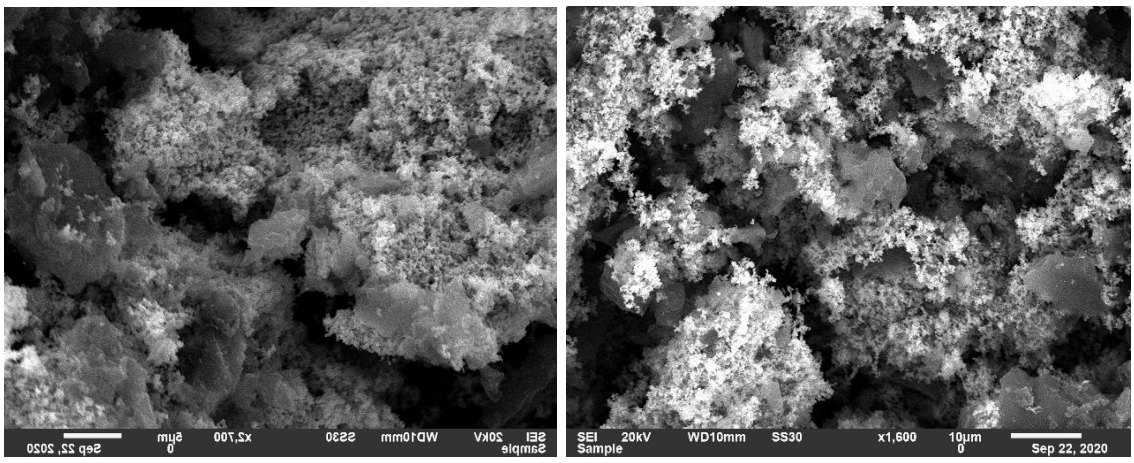

Figure 13: Scanning electron micrograph for ZnO@Ca-Alginate.

Figure (13) shows that the ZnO particles were supported to the alginate surface, which gives a proof about the success of composite formation**.**

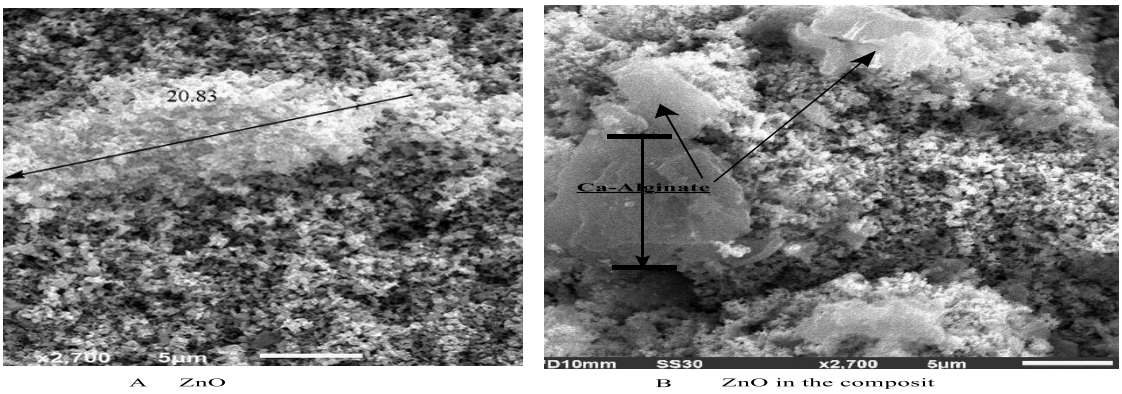

Figure 14: Scanning electron micrograph for :(A) commercial ZnO, (B) ZnO nanoparticles in the composite.

Figure (14 B) shows the presence of agglomerated ZnO NPs on the Ca-Alginate plates. The Ca-alginate plates sizes ranged from 4 to 7 µm. According to XRD particles size calculations, supported ZnO have smaller particles (~30 nm) comparing with naked one (~55 nm).

3.1.3 Energy Dispersive X-ray (EDX) Spectroscopy.

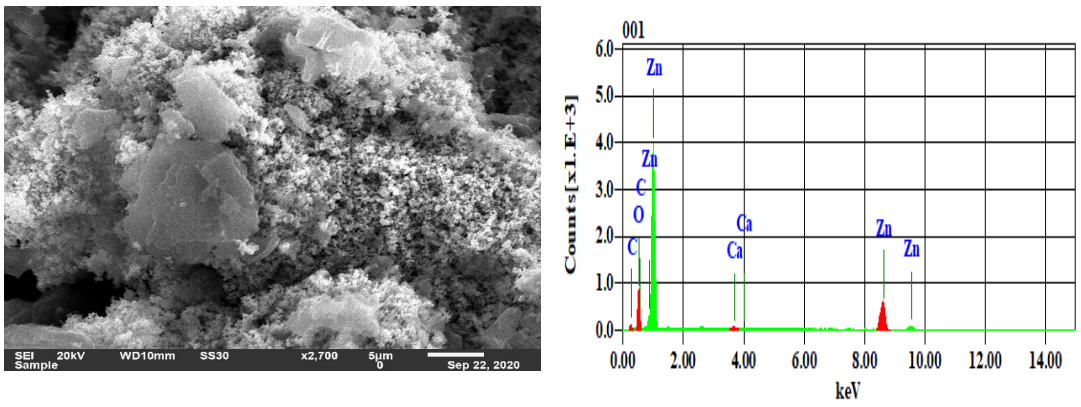

Figure 15: SEM and EDX spectra showing various elements in ZnO@Ca-Alginate.

EDX analysis was performed to indicate the incorporation of Ca-Alginate into composite, in addition to determine the elements identity and the percentage of each element in the composites. The presence of calcium, carbon, zinc, and oxygen elements that are constituents of the composite was confirmed by the spectrum as shown in Figure (15). The EDX analysis shows that the percentage of Zinc and oxygen are higher than carbon and calcium. This result is consistent with the ratio of the starting reactants concentrations in the reaction of composite preparation, in which it was in the ratio of (1:4) for Ca-Alginate and ZnO respectively.

Table (3) shows the EDX analysis results of the three analyzed spots in the composite sample. The quantity of C, O, Ca and Zn were shown. Details of the three EDX spectra of the catalyst values measured in atomic % was listed. The analysis results are approximately close together

Table 3: EDX weight of ZnO@Ca-Alginate nano composite using three spectrums focused three distinct areas.

ZnO/Ca-Alginate	Atomic %C	Atomic %O	Atomic %Ca	Atomic %Zn
Site 1	33.14	44.89	0.15	21.81
Site 2	30.27	43.56	0.39	25.78
Site 3	28.59	48.87	0.17	22.37
Average	30.6	45.7	0.24	23.3

3.1.4 Fourier-transform infrared spectroscopy (FT-IR) characterization

3.1.4.1 FT-IR for ZnO

The absorption band with a wavenumber ~480 cm^{1} in spectrum belongs to the Zn-O vibration mode [63]. Other insignificant bands at 1160 cm^{-1} and 1300 cm^{-1} were likely related to CO_2 absorbed from the air atmosphere and can therefore be neglected, see Figure (16)

Figure 16: FT-IR spectrum for ZnO.

3.1.4.2 FT-IR spectrum for Ca-Alginate

Alginic acid is a copolymer derived from 1,4-linked-b-D-mannuronic acid (M) and a-L-guluronic acid (G) [64] with two main bands of absorption associated with each polymer , as shown in Figure (17).

Figure 17: Alginic acid constituentations, where (A) is b-D-mannuronic acid and (B) is a-L-guluronic acid.

The band at 810 cm^{-1} in Figure (18 b) resulted from the vibration of mannuronic acid. Although guluronic acid's C-O stretching vibration resulted in a band absorbed at ~1030 cm^{-1}[49].

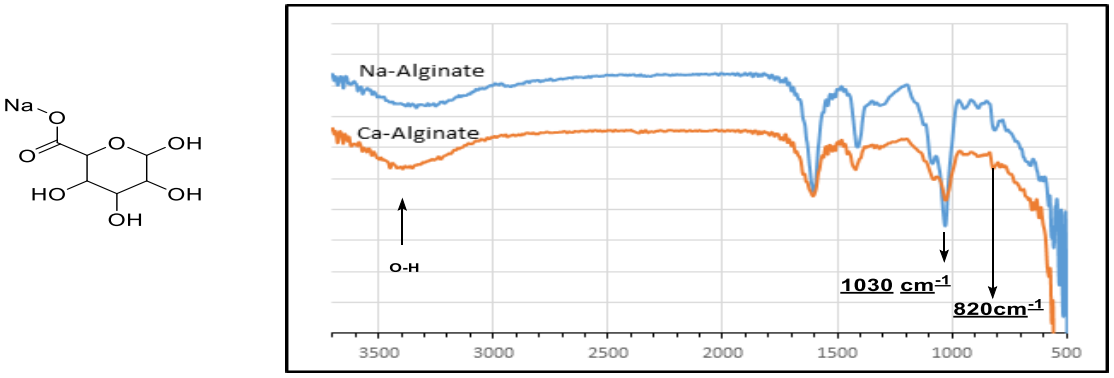

Figure 18 : FT-IR spectrum for (A) Sodium-Alginate, (B) Calcium-Alginate.

Compared with the infrared spectrum of the Na-Alg and Ca-Alg in Figure (18), the Ca-Alg absorption band related to O-H vibration around 3300 cm^{-1} appeared narrower than that of Na-Alg. The decreasing in hydrogen bonding resulted from Ca^{2+} crosslinking was responsible about the broadening decreasing. Shifting in vibration wave number for bands could be noticed since calcium ions form a chelating structure by participating in carboxyl and hydroxyl groups of alginates. The displacement occurs due to the substitution of Na^{+} with Ca^{2+}. Table (4)

Table 4: comparison between Ca-Alginate and Na-Alginate IR spectrum bands.

	-C-O (uronic acid)	O-C-O	C=O	O-H
Ca-Alg	1029 cm^{-1}	1420 cm^{-1}	1606 cm^{-1}	3392 cm^{-1}
Na-Alg	1031 cm^{-1}	1412 cm^{-1}	1604 cm^{-1}	3333 cm^{-1}

3.1.4.3 FT-IR spectrum for ZnO@Ca-Alginate

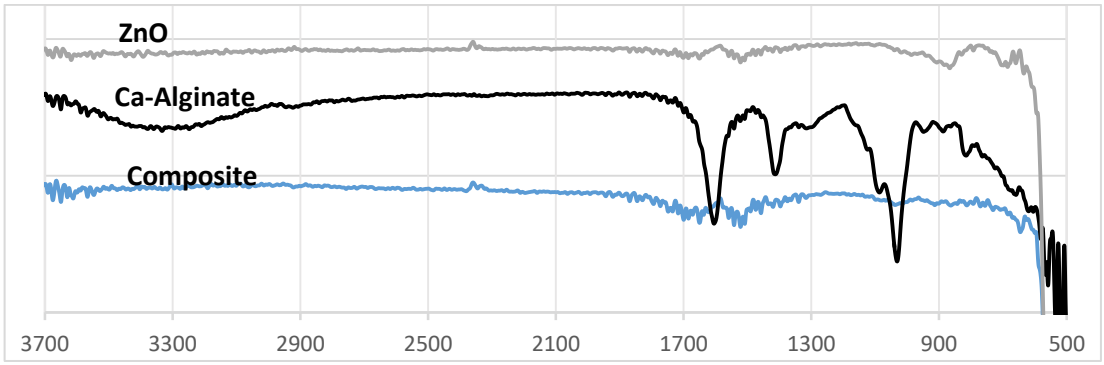

Figure 19 :IR spectrum for: (A) ZnO, (B) Ca-Alginate, (C) ZnO@Ca- Alginate.

The absorption bands of the ZnO@Ca-Alginate nanocomposites show the similarity of the absorption bands of Ca-alginate and nano ZnO with shifting in peaks position due to the chemisorption of alginate onto catalyst surface.

Vibrations at 1039, 1520 and 1650 cm^{-1} are attributed to Ca-Alginate. While the 520 cm^{-1} wave number is attributed to Zn-O vibration band. As shown in Figure (19). Nano Ca-alginate has been successfully modified with nano ZnO.

3.1.5 Thermal Studies.

3.1.5.1 TGA for ZnO

In Figure (20), The linearity of line expresses a high thermal stability.

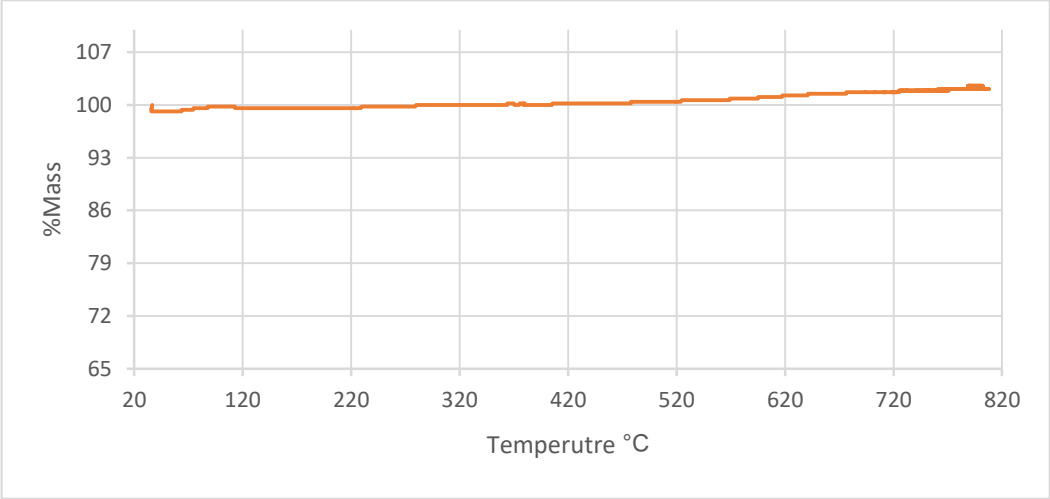

Figure 20: TGA plot for the thermal behavior of ZnO nanoparticles.

3.1.5.2 TGA for Ca-Alginate

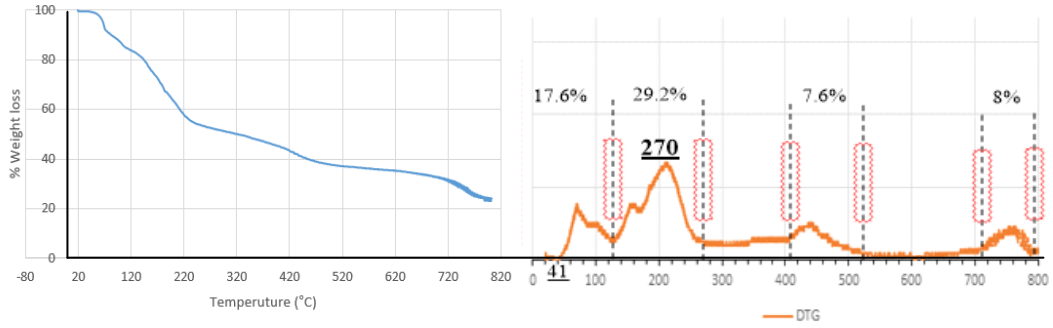

Figure 21: TGA/DTG plot for the thermal behavior of Ca-Alginate nanoparticles.

The loss of water molecules in alginate beads occurs in TGA studies at a temperature ranged 40 - 160 °C [65], Figure (21). The principle weight loss for Calcium alginate was in the temperature ranged 134 ºC - 266 ºC with a maximum at 270 ºC. The mass loss ~ (29.2%) is corresponding to

the complete decomposition of the alginate backbone structure. The remaining residue was ~ 23 %.

3.1.5.3 TGA of ZnO@Ca-Alginate

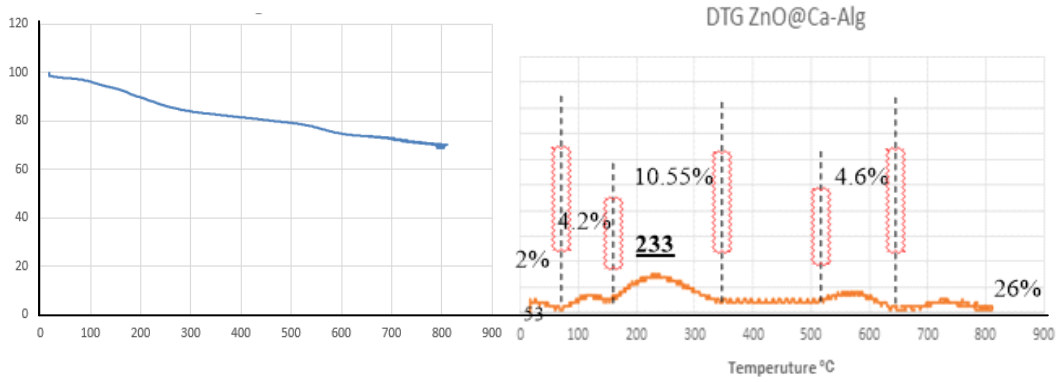

Figure 22: TGA & DTG plots of ZnO@Ca-Alginate nanoparticles.

Figure (22) shows the ZnO@Ca-Alginate nanocomposite TGA and DTG curves. The DTG curve showed three major thermal events. The first decomposition was in the temperature ranged from 41°C to 74 °C, this loses is attributed to the volatile components (like water molecules) and its value was ~ 2%. The decomposition of volatiles continues until it reaches up 97.5 °C with a mass loss of ~ 4.2% [66]. The second thermal event occurred at 154 °C with a mass loss of ~10.55 %. The third thermal event occurred at the temperature ranged 521- 635 °C with a mass loss ~ 4.6 %. The remaining residue was 68.65 %. Table (5).

Table 5: Thermal decomposition results of Ca-Alginate and the composite.

	First decomposition temperature	Highest decomposition temperature	Residual left
Ca-Alginate	41°C	220 °C	23%
ZnO@Ca-Alginate	53°C	233 °C	68.65%

The presence of ZnO in the alginate matrices raises the temperature of decomposition of the polymer from 220 to (233 ^{o}C). Several reports indicate that the presence of inorganic incorporation affects thermal stability of the polymers [67].

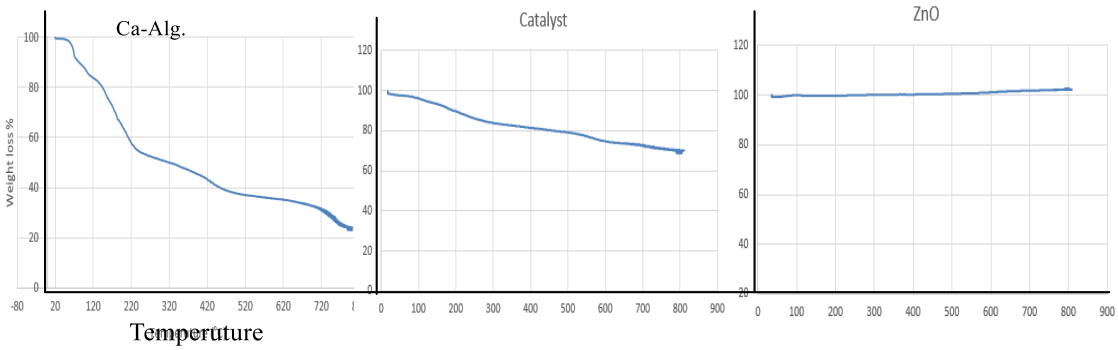

Figure 23: TGA plot for the thermal behavior of :ZnO, ZnO@Ca-Alginate and Ca-Alginate nanoparticles.

Figure (23) shows a high thermal stability of the composite in the presence of ZnO, and it's attributed to the strong interaction of ZnO particles in the alginate matrix which leads to improvement in the thermal stability of the compound [68]. The presence of ZnO nanoparticles leading to increasing the density of the surface that exposed to heat, and then protecting the bulk of the sample, and as a result reduces the rate of mass loss during the thermal decomposition of the composite.

3.2. Point of zero charges (Pzc)

Pzc is defined as the pH at which the net surface charge of the particles becomes zero [69].

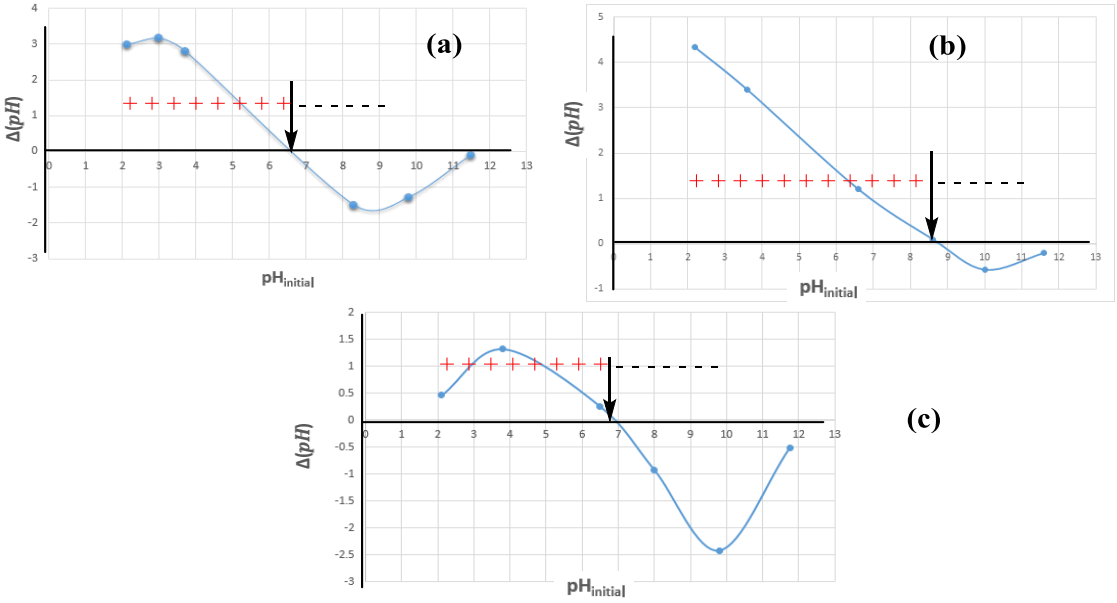

Figure 24: Plot of Δ(pH) vs. initial pH for: (a) Ca-Alginate, (b) ZnO and (c) ZnO@Ca-Alginate. Intercept shows value of Pzc for the solids.

Figure (24) shows the Pzc values for Ca-Alginate, ZnO and ZnO@Ca-Alginate. The Pzc values were ~ (6.5, 6.8 and 8.8) respectively. Pzc for commercial ZnO matched with similar study [11].

At pH values lower than Pzc, the surface of solids were positively charged. At pH values higher than Pzc, the surface of the solids was negatively charged.

MB has a cationic dye configuration and a pKa ~3.8 [70]. The surface charge of the catalyst and the equilibrium structure on the

contaminant molecules plays a main role in adsorption process. So that It is important to determine Pzc of the catalyst.

MB exists in cationic form (MB^+) in acidic medium and a neutral methylene blue violate (MBV) species in highly basic medium. The electrostatic repulsion will appear between the positive surface of the catalyst and the cationic MB at pH < Pzc [71]. On the other hand, the hydrogen bonding will be between the catalyst surface charge and the MBV neutral species, especially in which the alginate skeletal is rich in hydroxyl groups and the MB molecules contain nitrogen atom in the highly basic medium at pH > 9.5 [64]

At pH ~ 7.7, the catalyst begins to has a negative surface charge (based on Pzc). The surface charge density increases as the pH increases, while the MB is present as cationic species until pH 10. So the electrostatic attraction force is the main feature in the adsorption behavior.

MB in the more basic solution (High pH values > 10) produces a relatively stable neutral derivative Methylene violet (MVB) [72, 73], Figure (25 B). The H-bonding between the alginate hydroxyl groups and the nitrogen and oxygen atoms of the MBV will be the main adsorption mechanism, Figure (25) and (26).

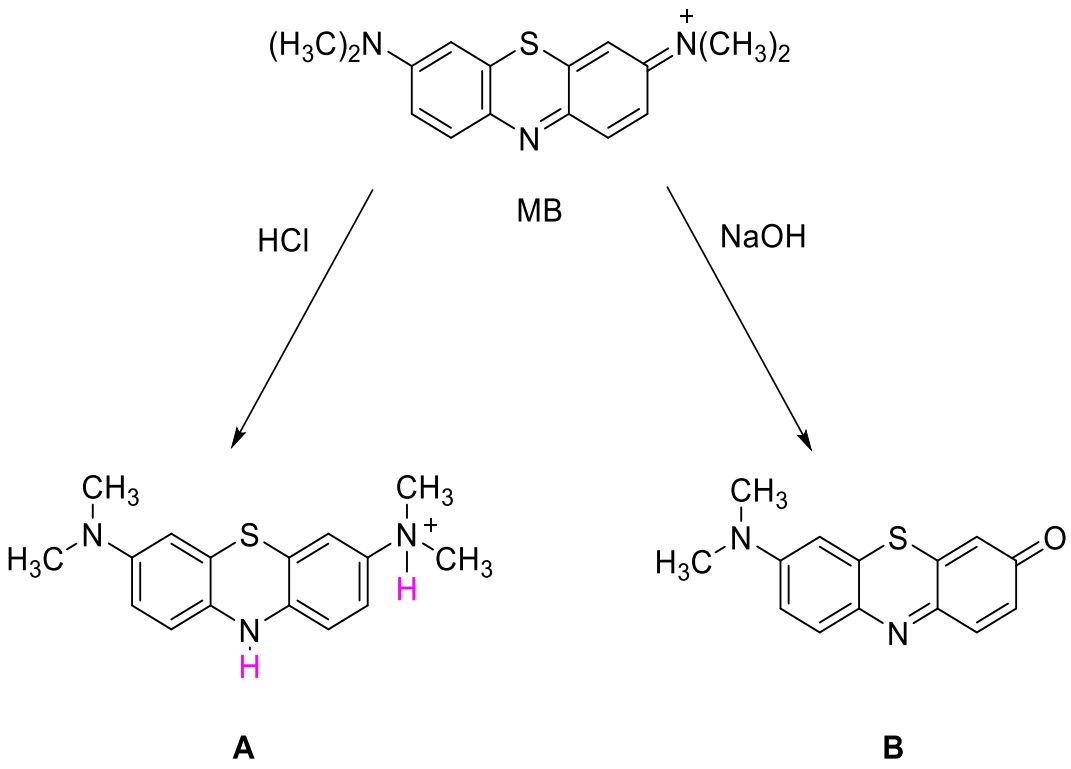

Figure 25: MB structure equilibrium (A) at low pH solution [69], (B) at high pH solution (MBV) [67].

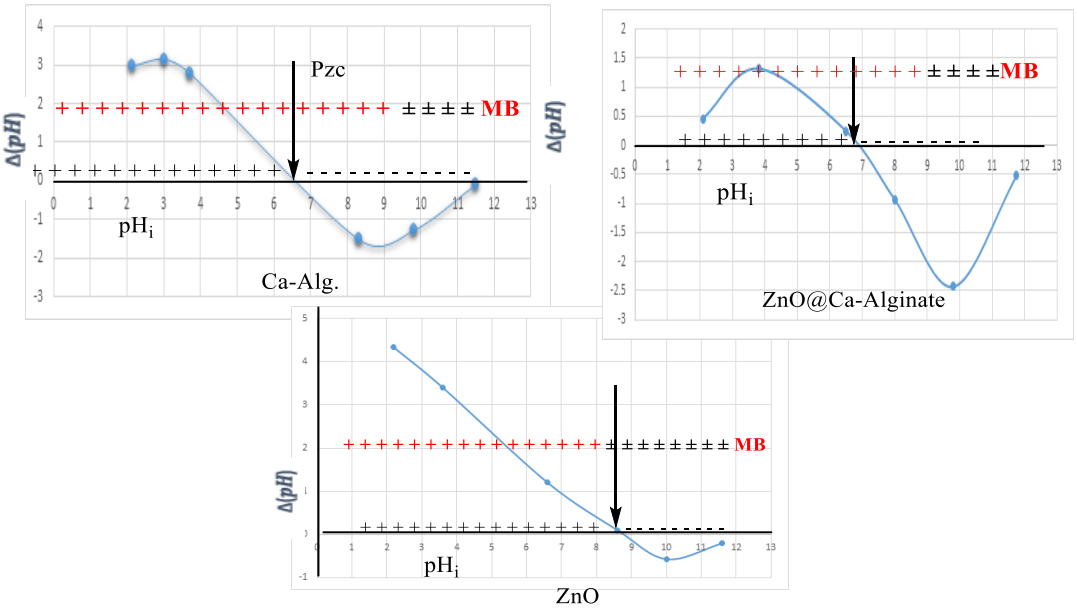

Figure 26: Plot of Δ(pH) vs. initial pH for for: (A) Ca-Alginate, (B) ZnO@Ca-Alginate (C) ZnO.

IM has two pKa values. Its equilibrium structure is mostly positive below pKa_1 and mostly negative above pKa_2, while it is mostly neutral at $pKa_1 < pH < pKa_2$. At the range of pH in which the catalyst surface charge is similar of opposite with the IM molecules charge, the electrostatic force will play the main feature in IM adsorption and then photodegradation. On the other hand, the H-bond will play the main feature of adsorption in the case of neutral equilibrium structure of IM, Figure (27).

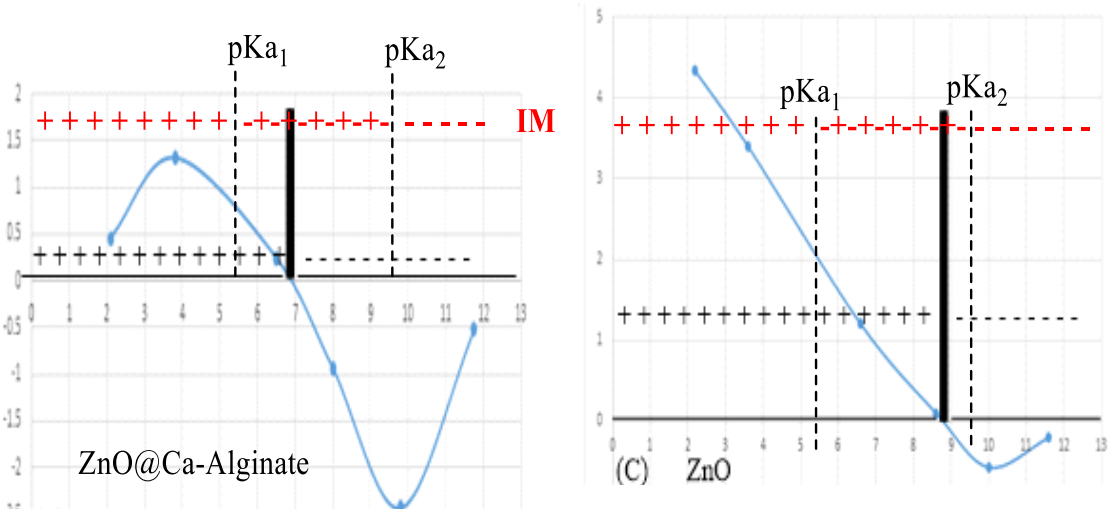

Figure 27: Comparison between the catalyst surface charge and IM surface charge.

3.3 Adsorption study

The chemical structure of Ca-Alginate and its functional groups are important for the adsorption process, in addition to its porosity and specific surface area.

3.3.1 MB adsorption onto Ca-Alginate.

Adsorption of MB (40 mL, 40 ppm) onto 0.10 g of Ca-Alginate was studied at different pH values ~ (3, 7.7, 10, 11, 12 and 13); the temperature

was thermostated at 30°C ± 5°C during the adsorption and photodrgadation process. The solution was stirred for 60 minutes in dark.

3.3.1.1 Effect of pH on MB adsorption onto Ca-Alginate.

One of the most important variables for dye adsorption was stated to be the solution pH.

Table 6: % Adsorption and amount of adsorbed of MB (40 mL, 40 ppm) on 0.10 g Ca-Alginate after 60 minutes at 30 °C± 5°C, at different pH values.

	After 60 minutes	
	% Ads	q_t (mg/g)
pH~3	20%	3.20
pH~7.7	60%	9.60
pH~10	67%	10.80
pH~11	52%	8.32
pH~12	45%	7.28
pH~13	15%	2.40

From Table (6), the adsorption efficiency increases as pH increases until it reaches pH 10, where it reaches its highest levels of efficiency. Above pH 10 that, the efficiency adsorption of the catalyst begins to decrease.

At pH ~3 the Ca-alginate is positively charged and the MB is present as cationic form, therefore the similarity of Ca-Alginate surface charge and the cationic form of MB will lower the amount of adsorbed MB.

At pH ~7.7 the Ca-alginate surface charge is negative, while the MB is mostly present in its cationic form. This difference in charges between

the MB and Ca-alginate surface will increase the amount of adsorbed MB molecules.

At pH~10 the catalyst has a high density of negative charge while the MB still has its cationic configuration, so an electrostatic attraction is expected to occur. At pH ~11, the electrostatic attraction force, in addition to H-bonding, participates in molecules adsorption. MB is present (mostly) in its produced neutral derivative MBV (at high pH values) besides the cationic configuration, so the H-bonding will play the main feature in the adsorption mechanism. The cationic form (MB^+) is present in small quantities and the Ca-alginate surface is highly-negatively charged at these pH, so that a stronger electrostatic attraction will interact with the cationic MB.

As pH increases > 11, the neutral MBV increases in concentration so the H-bonding will be the predominant mechanism. The H-bonding is weaker than the electrostatic attraction so the adsorption efficiency will decrease. The alginate is rich with hydroxyl groups and the MBV contains nitrogen atoms in addition to oxygen in which enables them to form H-bonding.

3.3.2 MB adsorption onto ZnO@Ca-Alginate (the composite).

A solution of MB (40 mL, 40 ppm) was stirred in the dark for 60 minutes with 0.10 g catalyst. Different parameters such as effect of contact time, effect of pH, and effect of MB concentrations were studied.

3.3.2.1 Effect of contact time on MB adsorption by ZnO@Ca-Alginate.

The effect of contact time of MB solution and the ZnO@CA-alginate mixture was studied. 0.10 g catalyst was stirred with MB (40 mL, 40 ppm) at pH ~7.7, and the temperature was thermostated at ~30°C ±5°C at time periods (0, 10, 15, 30, 60, 120 and 300 minutes).

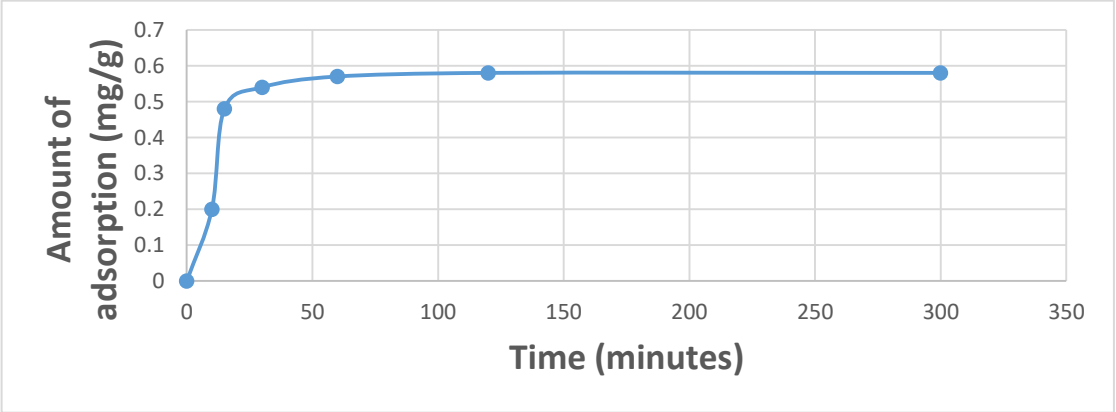

Figure 28: Effect of contact time on MB (40 mL, 40 ppm) adsorption by 0.10 g ZnO@Ca-Alginate; at 30°C ± 5°C and pH = 7.7.

Figure (28) shows the amount of adsorbed MB at different contact time periods. Initially the adsorption of MB was rapid, and this is attributed to the electrostatic attraction between the opposite charges of the catalyst surface and MB at pH ~7.7.

Later on we used 60 minutes as an adsorption equilibrium time in all of our adsorption experiments.

3.3.2.2 Effect of pH on MB adsorption by ZnO@Ca-Alginate.

Different pH values (~4, ~7.7,~10, ~11, ~12, and ~13) were adjusted for the solution to study the effect of pH on adsorption process after 60 minutes of stirring.

Table 7: Values of % Adsorption and amount of adsorbed MB. Measurements were made using MB (40 mL, 40 ppm), 0.10 g ZnO@Ca-Alginate after 60 minutes at 30°C ± 5°C with different pH values.

	After 60 minutes	
	% Ads	qt (mg/g)
pH~4	13%	2.08
pH~7.7	50%	8.00
pH~10	57%	8.80
pH~11	42%	6.80
pH~12	37%	6.00
pH~13	10%	1.60

As discussed above, at pH ~4 the composite catalyst surface is positively charged, and the MB is also presented in its cationic form, this similarity in charge will leading to electrostatic repulsion between the MB^+ and the composite catalyst surface.

At pH ~7.7 the catalyst surface is negatively charged and the MB is presented as a cationic form MB^+, this will produce an electrostatic attraction force, and this will increase the amount of adsorbed MB on the composite surface.

At pH ~ 10 the catalyst surface will be charged with a highly-density of negative charge. This will increase the electrostatic attraction with the cationic form of MB^{+}.

At pH >11 the formation of neutral derivative of MBV can also lower adsorption efficiency, and leads to the weaker H-bonding than electrostatic attraction Figure (29).

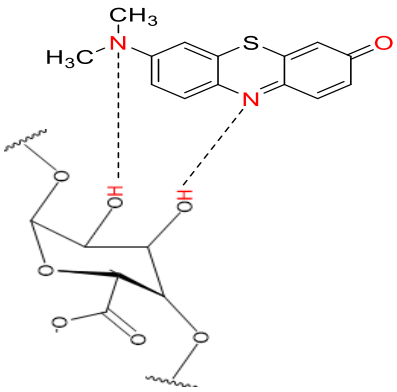

Figure 29: Possible MB hydrogen interaction with Ca-Alginate at high pH values.

In acidic medium the adsorption efficiency decreased dramatically. This is due to the electrostatic repulsion between the saturated positive charge of the catalyst surface and the cationic MB.

3.3.2.3 Effect of MB concentration on ZnO@Ca-Alginate adsorption.

An initial MB concentration of 20 and 40 ppm was investigated to study their effect on adsorption process after 60 minutes of stirring. The initial MB concentration is an essential factor because in the adsorption process, the solution concentration gives essential driving force needed for molecules to transfer between aqueous/solid phases [74]. A lowering in adsorption efficiency from 72% to 50% was observed when the

concentration of MB was increased from 20 to 40 ppm, Table (8). On the other hand, the amount of adsorbed MB (q_t) is approximately constant at different MB concentrations. This means that the adsorption capacity does not depend on the initial concentration but rather on the adsorption sites on the alginate surface.

Table 8: Effect of MB concentration on % Adsorption and the quantity of removal (qt). Measurements were made using MB (40 mL of 20 and 40 ppm), 0.10 g ZnO@Ca-Alginate after 60 minutes, at 30°C ± 5°C, pH ~7.7.

Time (min)	60 min.	
	%Ads	q_t(mg/g)
20 ppm	72%	0.576
40 ppm	50%	0.576

3.4 Photodegradation of MB:

A solution of MB (40 mL, 40 ppm) was mixed with 0.10 g catalyst at different pH and stirred in the dark for 30 minutes. Then the solution was exposed to solar simulated light lamp for 60 minutes at the default pH and temperature was thermostated to 30 °C ± 5 °C. A small amount of a liquate was taken every 15 minutes, centrifuged and then analyzed by UV-vis spectrophotometer. Different parameters as effect of pH, concentration of MB and concentration of catalyst were studied.

3.4.1 Effect of pH on MB photodegradation.

Different pH values ~ (4, 7.7, 10 and 11) of MB (40 mL, 40 ppm) mixed with 0.10 g catalyst were studied.

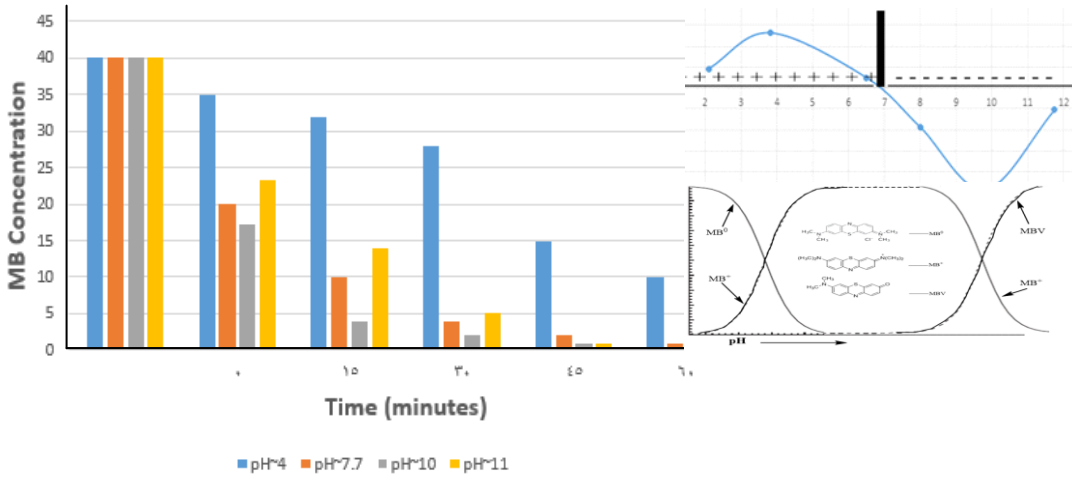

Figure 30: Effect of pH on MB solution (40 mL, 40 ppm) degradation reaction using 0.10 g of ZnO@Ca-Alginate.

Figure (30) shows that the photodegradation efficiency of MB increased as pH increases. MB photodegradation efficiency reached up to 98% at pH ~7.7 in 60 minutes. The maximum photodegradation efficiency was reached at pH ~10. As the photodegradation at 7.7 is approximately close to 100%. This pH (natural pH) was chosen here to complete our investigations.

As discussed before in the adsorption suction, at pH ~7.7 an electrostatic attraction is expected to occur between the MB^+ (cationic species) and the negatively charged composite surface (Pzc ~ 6.8).

At pH~10 an electrostatic attraction is expected to happen between the catalyst and the MB^+. The presence of NaOH will generate the reactive OH radicals which in turn will enhance the photodegradation efficiency. Therefore, efficiency of photodegradation increases with increasing the pH until it reaches the pH of 10 where it reaches the highest level of degradation efficiency. At pH > 10, the degradation efficiency of MB begins to decrease since neutral MBV (neutral species) is formed.

The H-bonding will be the predominant mechanism at pH range (> 10). Since H-bonding is weaker than electrostatic attraction, adsorption and photodegradation efficiency decreases.

On the other side, the degradation efficiency was lowered at low pH values. Only 75% contaminant loss occurred at pH ~4 after 60 min exposure to light. At pH ~4 the composite is positively charged, while the MB is present as cationic form. The electrostatic repulsion between the composite surface charge and the cationic form of MB lowers the amount of photodegraded MB.

Table 9: Effect of pH on values of T.N., T.F. and % Degradation. Measurements were made after 30 and 60 min, under direct simulated light using solution of MB (40 ml, 40 ppm) with 0.10 g composite (0.075 g ZnO).

30 min				60 min		
pH	%Deg	T.N($x10^{-3}$)	T.F($x10^{-3}$)	%Deg.	T.N($x10^{-3}$)	T.F($x10^{-3}$)
4	21%	1.1	0.037	75%	3.95	0.066
7.7	90%	4.70	0.157	98%	5.10	0.085
10	96%	5.03	0.167	100%	5.23	0.087
11	83%	4.37	0.146	95%	4.97	0.083

3.4.2 Effect of MB concentration on photodegradation

Concentrations of MB (10, 20, 30, 40 and 50 ppm) were studied. 40 mL of MB solution was mixed with 0.10 g catalyst; the mixture was stirred in dark for 30 min. and then exposed to light. Turnover number (T.N.), turnover frequency (T.F.) and degradation percentage were calculated after 60 min. as shown in table (10).

Table 10: Effect of MB concentration on values of overall rate, turnover number, turnover frequency and % Degradation. Measurement were made after 60 min, using 0.10 g ZnO@Ca-Alginate under solar simulated light, pH ~7.7, temperature = 30°C ± 5, volume = 40 mL.

MB (ppm)	% Degradation	T.N.×10^{-3}	T.F. × $10^{-3}$$min^{-1}$)
10	100	1.36	0.023
20	100	2.7	0.045
30	100	4.07	0.068
40	97	5	0.087
50	90	5.43	0.091

T.N. and T.F. values show an increase with increasing the MB concentration. The high concentration of pollutants gives it a greater opportunity to reach the active sites on the catalytic surface. That's gives a greater opportunity for the reactive types ($OH^{\bullet}$ and $O^{\bullet}$) to interact with MB and degrade it.

3.4.3 Effect of catalyst loading on MB photodegradation

The amounts of catalyst (0.05, 0.10, 0.20, 0.25 g) were studied by mixing a specific composite amount with MB (40 mL, 40 ppm). The pH was adjusted to ~7.7 and at the temperature was thermostated to 30°C ±5.

First, the % Degradation increased with increasing the amount of the composite as shown in Table (11). At higher loading, the efficiency and the T.N. were lowered, because higher number of catalyst particles blocks the light from the surface of the catalyst [75]**.** The 0.10 g was found to be the optimal catalyst quantity. It showed a high degradation percentage with a high T.N.

Table 11: Effect of catalyst loading on values of T.N., T.F., and % Degradation for MB. Measurements were made after 60 minutes using 0.10 g ZnO@Ca-Alginate under solar simulated light, pH ~7.7, temperature = 30°C ±5, contaminants (40 mL, 40 ppm).

Catalyst weight (g)	% Degradation	T.N. × 10^{-3}	T.F. × 10^{-3}
0.05	65	6.50	0.110
0.10	97	5.00	0.084
0.20	95	2.58	0.043
0.28	92	1.76	0.030
0.35	91	1.30	0.021

3.5 Comparison between commercial ZnO and ZnO@Ca-Alginate in photodegradation of MB

Tow solutions of MB (40 mL, 40 ppm) were prepared. A 0.10 g ZnO@Ca-Alginate was added to first solution, to the second solution 0.08 g ZnO was added. The two solutions were stirred in dark for 30 minutes at pH ~7.7 and at temperature 30°C ±5. After that, the solutions were exposed to simulated solar light for 60 minutes. The remaining MB was measured by UV-spectrophotometer. The photodegradation results are shown in Figure (31).

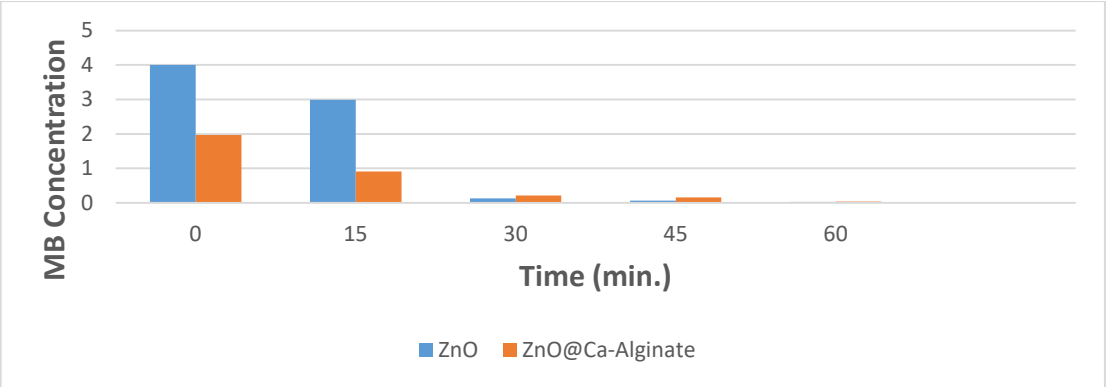

Figure 31: Comparison between (0.08 g) ZnO and (0.10 g) ZnO@Ca-Alginate in MB degradation. Measurements were made using MB concentration (40 ppm), solution volume=40 mL, pH ~7.7, temperature = 30°C±5

Figure (31) shows that the ZnO@Ca-Alginate has higher adsorption efficiency of ~50% at zero-time irradiation (before irradiation), while the ZnO has lower adsorption efficiency toward MB. Both of naked ZnO and composite show high photodegradation efficiency after more than 30 minutes of irradiation. Therefore, the composite system does not increase photodegradation, but has the advantage of easy catalyst separation.

3.6 IM adsorption onto ZnO@Ca-Alginate

A solution of IM (50 mL, 20 ppm) was mixed with 0.10 g composite ZnO@CA-Alginate. The effect of pH on the IM adsorption was studied. The solution of IM was adjusted at different pH values ~ (4.5, 7, 9 and 12) and stirred for 60 min, no significant adsorption was observed at all pH values for IM on the composite.

3.7 IM photodegradation study.

A solution of IM (50 mL, 20 ppm) was mixed with 0.10 g catalyst in a 250 mL beaker, stirred in the dark for 30 minutes then irradiated by using simulated solar light lamp (Philips, low voltage halogen lamp, 36V and 400 W) with alight intensity of ~100000 lux (similar to the intensity of the natural sunlight) over 2-hour. Aliquots were withdrawn periodically at different time periods, centrifuged and analyzed by using HPLC, the absorption wavelength of IM~ 273 nm. Effect of pH on photodegradation was also studied.

3.7.1 Effect of pH on IM photodegradation using ZnO@Ca-Alginate.

Diluted solutions of HCl and NaOH were used for adjust the pH of IM solution, values of OM solution pH were adjusted to the following pH values ~ (4.5, 7, 9, and 12).

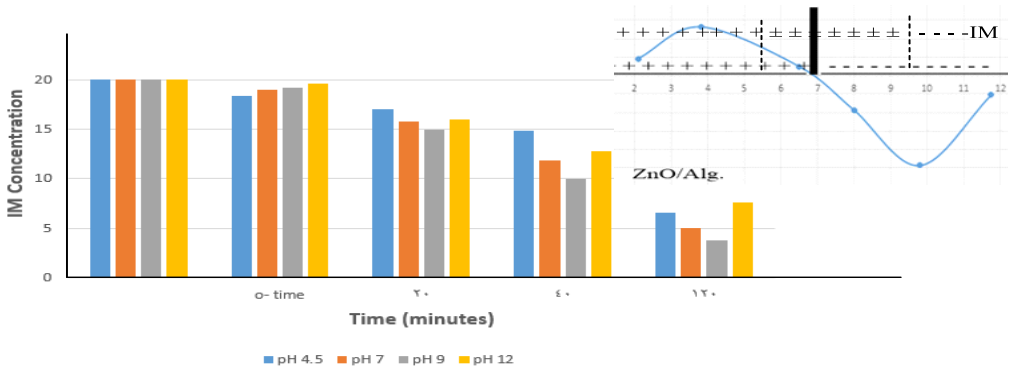

Figure 32: Effect of pH on IM (50 mL, 20 ppm) degradation efficiency using 0.10 g of ZnO@Ca-Alginate.

As shown in Figure (32), the higher photodegradation efficiency of IM was at pH ~9, so that the pH ~ 9 was chosen as default pH for further IM photodegradation experiments. The solution, at pH 9, is rich with OH^- which is the main source of $^{\bullet}OH$ (the mostly active species in the photodegradation process). This feature can explain the increasing of IM photodegradation at such pH value.

IM is mostly present as a neutral form at pH range (5.5< pH <9.5). Therefore, at this pH range the hydrogen bonding is expected to be the predominant adsorption mechanism rather than electrostatic attraction, Figure (33).

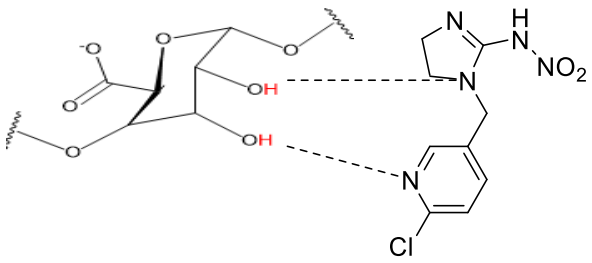

Figure 33: Possible IM hydrogen interaction with Ca-Alginate.,

At pH ~7 the H-bonding is still the predominant mechanism between the neutral IM molecules and the surface negatively charged composite. The photodegradation efficiency is predicted to be less than at pH ~9. This may also be due to lowering of OH^- ions in the neutral solution compared with basic solution at pH = 9.

At pH ~12, both the IM molecules and the composite surface are present in the negative ionic forms. The similarity in charge between the IM and the composite surface causes electrostatic repulsions, which keep

the IM molecules far away from the catalyst surface. This lowers the photodegradation process of IM.

At low pH value (~4.5), the IM is present as a positively charged species, at the same time the composite catalyst surface is positively charged. The charge similarity between IM and the composite surface will produce a repulsion forces that keep the IM molecules far away from the catalyst surface. A lowering in the photodegradation of IM will thus occur.

3.8 Confirmation of contaminant mineralization.

HPLC analysis was done after different periods of irradiation, to study the degradation process intermediate. The lowering in the contaminant peak area and the formation of new peaks (intermediates) confirmed contaminants degradation.

3.8.1 HPLC for MB

HPLC analysis was performed for a solution of MB. A solution of MB (40 mL, 40 ppm) was mixed with 0.10 g catalyst. Aliquots where syringed out of the mixture at different irradiation time periods (0, 30, 90, 120 and 140 minutes), the syringed liquates were centrifuged and analyzed by HPLC (Water1525) at 663 nm.

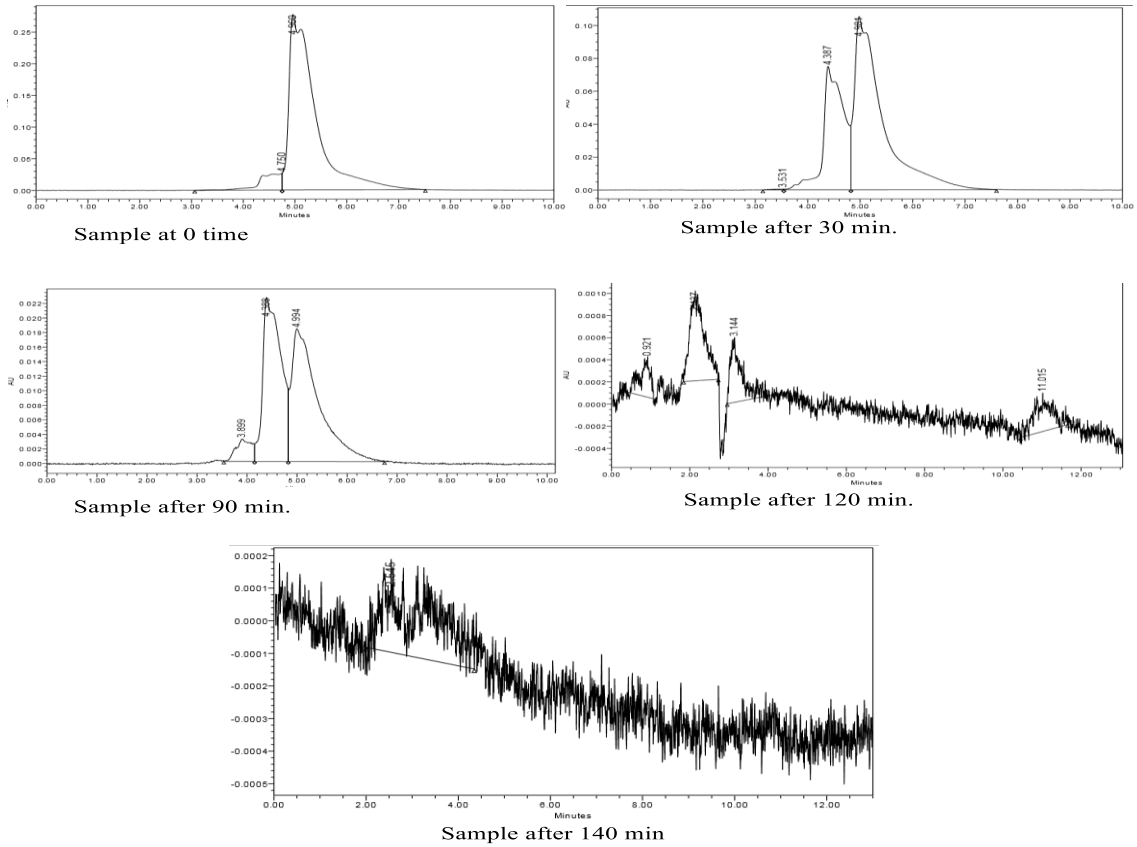

Figure 34: HPLC absorbance chromatogram for sample of 40 mL MB (40 ppm) mixed with 0.10 g catalyst at different times interval.

Figure (34) shows that two peaks with retention time at ~ (4.3 and 5 min) were observed. The peak with retention time ~ 5 min refers to the MB. The peak area of MB decreased while the intermediate's peaks increased with time until It's completely mineralized to CO_2, H_2O and inorganic gases which are expected to be SO_4, NH_3 and nitrate/nitrite ions within 120 minutes [76]. Peak 2, which resulted during the photodegradation process and appeared at retention time 4.3 min, first increased gradually during photodegradation; but at the end of the photodegradation process the two peaks almost completely disappeared. This confirms complete degradation of any original or produced organic species during the photdegradation process. As shown in Figure (35).

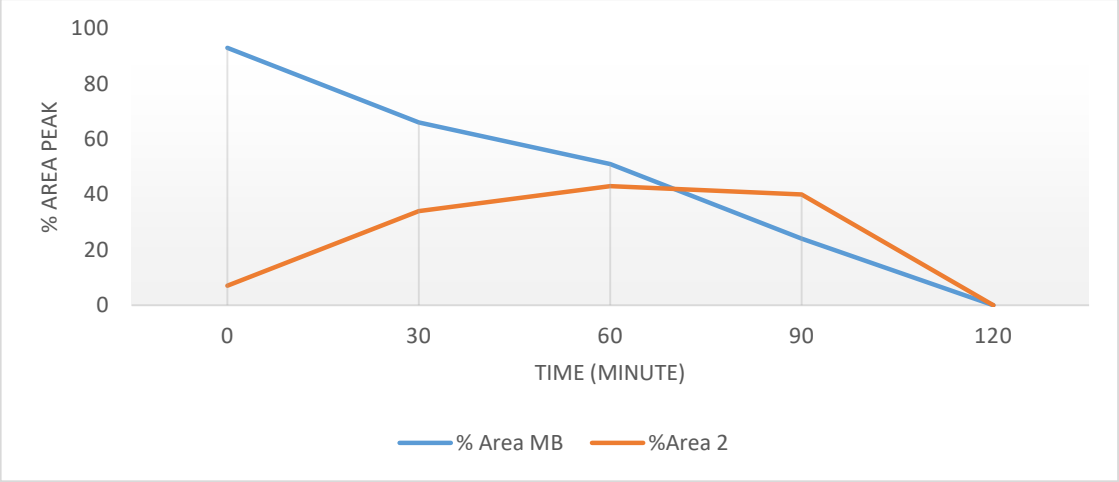

Figure 35: HPLC absorbance chromatogram of the peaks area for MB degradation

3.8.1.1 Analysis of produced inorganic minerals during the photodegradation of MB:

A Nessler reagent was used for NH_4^+ ion detection [54]. Cadmium reagent was used for detection of the NO_3^- ions [55] and barium chloride solution was used for detection of the SO_4^{-2} ions [56] after the photodegradation experiments. The analysis results for possible inorganic minerals for the photodegradation of MB are presented in Table (12)

Table 12: Concentrations of inorganic ion that resulted from photodegradation of MB. Measurement were made using MB solution (40 mL, 40 ppm) mixed with 0.10 g at two photodegradation times periods.

Ions	60 minutes	120 minutes
SO_4^{-2}	Not detected	Not detected
NH_4^+	4 ppm	Not detected
NO_3^-	1.77 ppm	3.5 ppm (~1 ppm as N)

The carbon in the dye molecules was converted into carbon dioxide, while the sulfur and nitrogen end up as inorganic ions such as sulfate, ammonium and nitrate ions.

As shown in Table (12), the amount of sulfate (SO_4^{2-}) is less than the expected from the initial MB concentration. This is possibly due to adsorption of sulfate ions on the composite surface [41]. The N atoms begin to form unstable ammonium cations (NH_4^+), which gradually transform into more stable nitrate ions. After 120 min of irradiation, only ~ 3.5 ppm of NO_3^- was detected (with ~1 ppm N), while the value of produced nitrogen in the solution from photodegradation of 40 ppm of MB should be ~6 ppm. The difference in values is attributed to conversion of parts of nitrogen contents into N_2 gas or possible escape of the ammonium as NH_3 gas.

3.8.2 HPLC analysis of the photodegraded IM solution.

A solution of IM (50 mL, 20 ppm) was mixed with 0.10 g catalyst. Aliquots of solution where syringed out at different time periods (0, 90, 320 and 440 minutes). The aliquots were centrifuged and analyzed using HPLC (Water1525) at 270 nm.

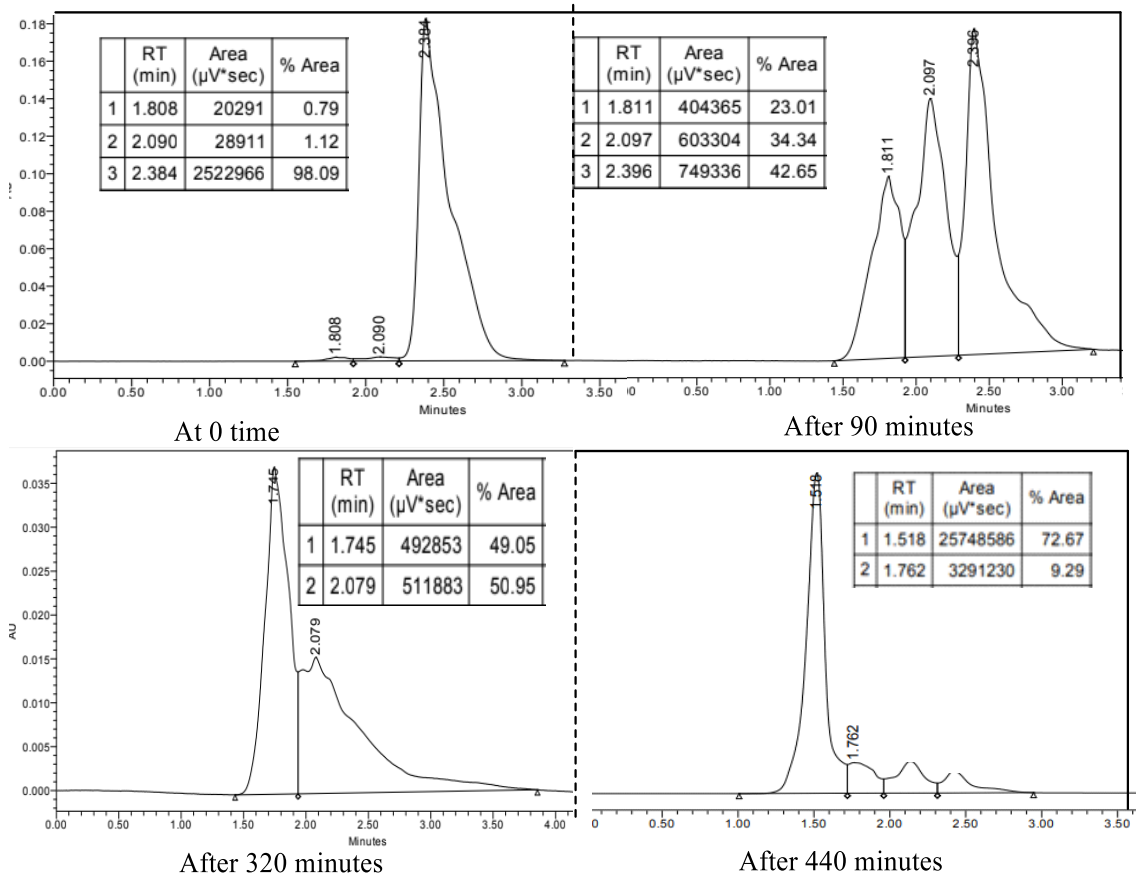

Figure 36: HPLC absorbance chromatogram for a solution of IM (50 mL, 20 ppm) mixed with 0.10 g catalyst for different times (0,90, 320 and 440 minutes) at pH 9 and at temperature 30°C ±5.

Figure (36) illustrates three probable intermediate compounds produced during the photodegradation of IM [77]. The three peaks have retention times (~2.4, 2.1 and 1.8 min). The peak with retention time ~ 2.4 min is referred to IM. The other two peaks are attributed to the produced intermediate species.

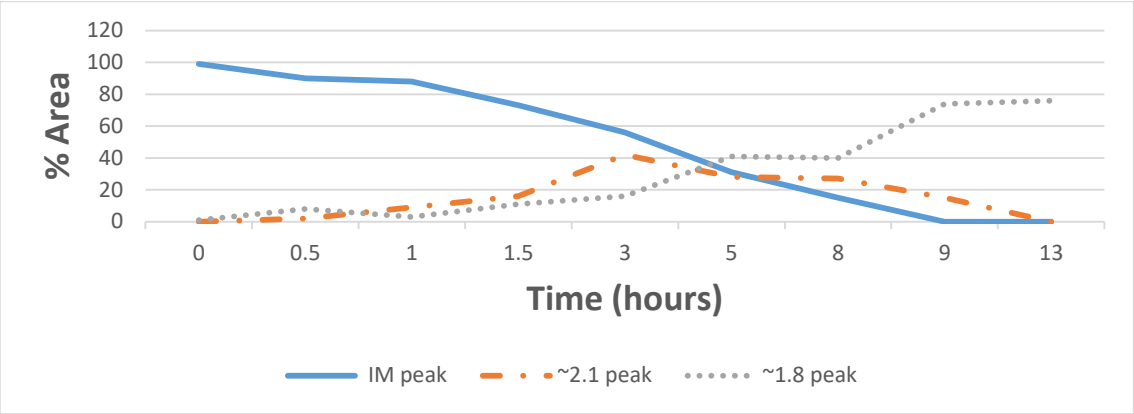

Figure 37: HPLC absorbance chromatogram of the peaks% area for IM degradation.

Figure (37) shows that there is a decrease in the IM concentration with time. The peak with a retention time of 2.1 min increased at first period of photodegrradtion process and then started to fall down at the end of photodegradrtion course. This peak is attributed to intermediate species. The peak at retention time of ~1.8 min, may be attributed to the produced chloride ions which gradually increased during the photodegradation of IM [78]. The final products of photocatalytic degradation of IM are CO_2, Cl^- and NO_3^- [79].

When the technical IM was used in other studies [80] at the same initial concentration, the rate of degradation was faster. This is expected because it does not contain competing additives and stabilizers.

3.9 Catalyst reuse

The photodegraded MB solution was decanted, the remaining composite was taken, washed and the solution was decanted again. A fresh solution of MB (40 mL, 40 ppm) was added to the composite, the mixture was stirred and exposed to source of irradiation for 60 min. The solution

was then spectrophotometrically analyzed to determine the amount of the remaining MB. The results are shown in Table (13). The percentage of degradation for recovered catalyst was determined. No significant lowering was observed in the catalyst efficiency on reuse.

Table 13: Values of % Degradation of MB using recovered ZnO@Ca-Alginate catalyst

Trial	% Degradation
1	98%
2	97%

3.10 Conclusions

1. Alginate demonstrated a high capacity for adsorption at various pH levels despite the small amount involved in forming the composite in the case of methylene blue, while it showed no adsorption efficiency in case of IM.

2. The composite had higher photodegradation efficiency in the case of methylene blue (100%) and lower efficiency in the case of imidacloprid.

3. Commercial ZnO showed larger particle size and smaller agglomerates than supported one.

4. The point of zero charge (Pzc) of ZnO, Ca-Alginate and ZnO @ Ca-Alginate (8.7, 6.5 and 6.8 respectively) was determined using the pH drift method.

5. Thermal stability for ZnO, Ca-Alginate and ZnO@Ca-Alginate was measured using the TGA method and found that composite was more thermal stability than Ca-Alginate.

6. The adsorption and degradation of contaminants are affected by the pH solution, the charge of the contaminants, and the surface charge of the catalyst (Pzc).

7. The optimum pH value for contaminants photodegradation by ZnO@Ca-Alginate was ~7.7 (nature) for MB and ~ 9 for IM.

8. The experimental data showed that increasing the concentration of contaminants causes an increase in the amount of its removal by composite.

9. The experimental data showed that the equilibrium time for adsorption of MB by Ca-Alginate could be taken after approximately 60 minutes.

3.11 Recommendations for future work

1. Using the point of zero charge values of many adsorbents (ZnO, Ca-Alginate, ZnO@Ca-Alginate) as references in removing other pollutants through adsorption and light degradation.

2. Examine the influence of other factors that may affect the adsorption of Ca-Alginate, such as: temperature, and concentration of adsorbent in the compound.

3. Additional characterization for intermediates which formed from degradation, such as the use of mass spectrum and atomic absorption spectroscopy to analyze their elements.

4. Study ability to reuse ZnO for more than 2 times in photodegradation

References

1. A.H. Zyoud, M. Dwikat, S. Anabtawi, R. Alkowni, N. Qamhieh, A. Hajamohideen, S.H. Zyoud, M.H. Helal, S.H. Zyoud, H. Nassar, **Zinc Oxide in Photocatalytic Removal of Staphylococcus aureus and Klebsiella pneumoniae from Water with Ultraviolet and Visible Solar Radiations**, JOM, 73 (2021) 420-431.

2. P. Muthirulan, M. Meenakshisundararam, N. Kannan, ***Beneficial role of ZnO photocatalyst supported with porous activated carbon for the mineralization of alizarin cyanin green dye in aqueous solution***, **Journal of advanced research,** 4 (2013) 479-484.

3. W.H. Organization, **Preventing diarrhoea through better water, sanitation and hygiene: exposures and impacts in low-and middle-income countries,** World Health Organization, 2014.

4. S.W. Krasner, H.S. Weinberg, S.D. Richardson, S.J. Pastor, R. Chinn, M.J. Sclimenti, G.D. Onstad, A.D. Thruston, O**ccurrence of a new generation of disinfection byproducts**, Environmental science & technology, 40 (2006) 7175-7185.

5. S.-L. Loo, A.G. Fane, T.-T. Lim, W.B. Krantz, Y.-N. Liang, X. Liu, X. Hu, **Superabsorbent cryogels decorated with silver nanoparticles as a novel water technology for point-of-use disinfection**, Environmental science & technology, 47 (2013) 9363-9371.

6. A. Zyoud, M. Dwikat, S. Al-Shakhshir, S. Ateeq, J. Shteiwi, A. Zu'bi, M.H. Helal, G. Campet, D. Park, H. Kwon, ***Natural dye-sensitized ZnO nano-particles as photo-catalysts in complete degradation of E. coli bacteria and their organic content,*** **Journal of Photochemistry and Photobiology A: Chemistry**, 328 (2016) 207-216.

7. A.H. Zyoud, M. Dwikat, S. Al-Shakhshir, S. Ateeq, J. Ishtaiwa, M.H. Helal, M. Kharoof, S. Alami, H. Kelani, G. Campet, **ZnO nanoparticles in complete photo-mineralization of aqueous gram negative bacteria and their organic content with direct solar light**, Solar Energy Materials and Solar Cells, 168 (2017) 30-37.

8. A. Zyoud, R. Alkowni, O. Yousef, M. Salman, S. Hamdan, M.H. Helal, S.F. Jaber, H.S. Hilal, **Solar light-driven complete mineralization of aqueous gram-positive and gram-negative bacteria with ZnO photocatalyst**, Solar Energy, 180 (2019) 351-359.

9. L. Jiao, P. Qi, Y. Liu, B. Wang, L. Shan, ***Fe3O4 nanoparticles embedded sodium alginate/PVP/calcium gel composite for removal of Cd2+,*** **Journal of Nanomaterials**, 2015 (2015).

10. A. Zyoud, W. Jondi, N. AlDaqqah, S. Asaad, N. Qamhieh, A. Hajamohideen, M.H. Helal, H. Kwon, H.S. Hilal, **Self-sensitization of tetracycline degradation with simulated solar light catalyzed by ZnO@ montmorillonite**, Solid State Sciences, 74 (2017) 131-143.

11. A.H. Zyoud, A. Zubi, S.H. Zyoud, M.H. Hilal, S. Zyoud, N. Qamhieh, A. Hajamohideen, H.S. Hilal, **Kaolin-supported ZnO nanoparticle catalysts in self-sensitized tetracycline photodegradation: zero-point charge and pH effects,** Applied Clay Science, 182 (2019) 105294.

12. A. Zyoud, T. Zorba, M. Helal, S. Zyoud, N. Qamhiya, A. Hajamohideen, S. Zyoud, H. Hilal, ***Direct sunlight-driven degradation of 2-chlorophenol catalyzed by kaolinite-supported ZnO***, **International Journal of Environmental Science and Technology**, 16 (2019) 6267-6276.

13. A.H. Zyoud, S. Asaad, S.H. Zyoud, S.H. Zyoud, M.H. Helal, N. Qamhieh, A. Hajamohideen, H.S. Hilal, ***Raw clay supported ZnO nanoparticles in photodegradation of 2-chlorophenol under direct solar radiations,*** **Journal of Environmental Chemical Engineering**, 8 (2020) 104227.

14. W.H. Glaze, J.-W. Kang, D.H. Chapin, **The chemistry of water treatment processes involving ozone,** hydrogen peroxide and ultraviolet radiation, (1987).

15. I.E. Kochevar, **Basic concepts in photobiology, in: Photoimmunology**, Springer, 1983, pp. 5-21.

16. H. Matare, ***Carrier transport at grain boundaries in semiconductors***, **Journal of applied physics,** 56 (1984) 2605-2631.

17. N. Al Armouzi, M. Manoua, G. El Hallani, H.S. Hilal, A. Liba, N. Kouider, M. Mabrouki, **Effects of Sn Doping on Properties of Multilayered ZnO Films Deposited by Spin Coating/Sol–Gel Method**, JOM, 73 (2021) 411-419.

18. A. Jha, H.-G. Duan, V. Tiwari, M. Thorwart, R.D. Miller, **Origin of poor doping efficiency in solution processed organic semiconductors,** Chemical science, 9 (2018) 4468-4476.

19. B. Zhi, Y. Yang, N.V. Hudson-Smith, U.R. Kortshagen, C.L. Haynes, **Bacterial Toxicity of Germanium Nanocrystals Induced by Doping with Boron and Phosphorus**, ACS Applied Nano Materials, 2 (2019) 4744-4755.

20. S. Huang, G. Schlichthörl, A. Nozik, M. Grätzel, A. Frank, ***Charge recombination in dye-sensitized nanocrystalline TiO2 solar cells***, The **Journal of Physical Chemistry** B, 101 (1997) 2576-2582.

21. A. Goetzberger, E. Klausmann, M. Schulz, **Interface states on semiconductor/insulator surfaces,** Critical Reviews in Solid State and Material Sciences, 6 (1976) 1-43.

22. K. Nakata, A. Fujishima, ***TiO2 photocatalysis: Design and applications,*** **Journal of photochemistry and photobiology C:** Photochemistry Reviews, 13 (2012) 169-189.

23. J.C. Byers, S. Ballantyne, K. Rodionov, A. Mann, O. Semenikhin, **Mechanism of recombination losses in bulk heterojunction P3HT: PCBM solar cells studied using intensity modulated photocurrent spectroscopy,** ACS applied materials & interfaces, 3 (2011) 392-401.

24. H.O. Finklea, **Semiconductor electrodes**, (1988).

25. S. Kansal, M. Singh, D. Sud, ***Studies on photodegradation of two commercial dyes in aqueous phase using different photocatalysts***, **Journal of hazardous materials,** 141 (2007) 581-590.

26. A.H. Zyoud, F. Saleh, M.H. Helal, R. Shawahna, H.S. Hilal, ***Anthocyanin-sensitized TiO2 nanoparticles for phenazopyridine photodegradation under solar simulated light,*** **Journal of Nanomaterials**, 2018 (2018).

27. A.H. Zyoud, A. Zubi, S. Hejjawi, S.H. Zyoud, M.H. Helal, S.H. Zyoud, N. Qamhieh, A. Hajamohideen, H.S. Hilal, ***Removal of acetaminophen from water by simulated solar light photodegradation with ZnO and TiO2 nanoparticles: Catalytic efficiency assessment for future prospects,*** **Journal of Environmental Chemical Engineering**, 8 (2020) 104038.

28. A.H. Zyoud, H. Salah, S.H. Zyoud, S.H. Zyoud, M.H. Helal, N. Qamhieh, A. Hajamohideen, H. Nassar, H.S. Hilal, **ZnO-Based Catalyst for Photodegradation of 2-Chlorophenol in Aqueous Solution Under Simulated Solar Light Using a Continuous Flow Method**, JOM, (2020) 1-7.

29. C.-P. Chen, S.-H. Chan, T.-C. Chao, C. Ting, B.-T. Ko, ***Low-bandgap poly (thiophene-phenylene-thiophene) derivatives with broaden absorption spectra for use in high-performance bulk-heterojunction polymer solar cells***, **Journal of the American Chemical Society**, 130 (2008) 12828-12833.

30. A. Dhakshinamoorthy, H. Garcia, Catalysis by metal nanoparticles embedded on metal–organic frameworks, Chemical Society Reviews, 41 (2012) 5262-5284.

31. D. Narayanan, R. Jayakumar, K. Chennazhi, **Versatile carboxymethyl chitin and chitosan nanomaterials: a review,** Wiley Interdisciplinary Reviews: Nanomedicine and Nanobiotechnology, 6 (2014) 574-598.

32. S. Al-Musa, D.A. Fara, A. Badwan, ***Evaluation of parameters involved in preparation and release of drug loaded in crosslinked matrices of alginate***, **Journal of controlled release**, 57 (1999) 223-232.

33. Z. Ahmad, R. Pandey, S. Sharma, G. Khuller, ***Alginate nanoparticles as antituberculosis drug carriers: formulation development, pharmacokinetics and therapeutic potential***, **Indian journal of chest diseases and allied sciences**, 48 (2006) 171.

34. S. Sangeetha, D.N. Venkatesh, R. Adhiyaman, K. Santhi, B. Suresh, ***Formulation of sodium alginate nanospheres containing amphotericin B for the treatment of systemic candidiasis***, **Tropical Journal of Pharmaceutical Research**, 6 (2007) 653-659.

35. L. Li, Y. Fang, R. Vreeker, I. Appelqvist, E. Mendes, **Reexamining the egg-box model in calcium− alginate gels with X-ray diffraction**, Biomacromolecules, 8 (2007) 464-468.

36. D. Kühbeck, J. Mayr, M. Häring, M. Hofmann, F. Quignard, D.D. Díaz, ***Evaluation of the nitroaldol reaction in the presence of metal ion-crosslinked alginates***, **New Journal of Chemistry**, 39 (2015) 2306-2315.

37. A.S. Travis, **Heinrich Caro at Roberts**, Dale & CO, Ambix, 38 (1991) 113-134.

38. A.G. Gilani, T. Ghorbanpour, M. Salmanpour, ***Additive effect on the dimer formation of thiazine dyes,*** **Journal of Molecular Liquids**, 177 (2013) 273-282.

39.[39] A.L. Kellermann, S.S. Jones, **What it will take to achieve the as-yet-unfulfilled promises of health information technology**, Health affairs, 32 (2013) 63-68.

40.[40] V.V. Tkach, M.V. Kushnir, S.C. de Oliveira, A. Verbovetska, A.P. Kusyak, N.V. Kusyak, I.M. Dytynchenko, A.O. da Silva, P.I. Yagodynets, ***The theoretical description for methylene blue electrochemical determination and decolorization, assisted by polynaphthoquinones/Ti/TiO2/VO (OH) composite***, **Applied Journal of Environmental Engineering Science**, 6 6-1 (2020) 2014-2021.

41.[41] J.-M. Herrmann, **Water treatment by heterogeneous photocatalysis, in: Environmental catalysis**, World Scientific, 1999, pp. 171-194.

42. J. Cenens, R. Schoonheydt, **Visible spectroscopy of methylene blue on hectorite, laponite B, and barasym in aqueous suspension**, Clays and Clay Minerals, 36 (1988) 214-224.

43. K.Y. Jacobs, R.A. Schoonheydt, ***Spectroscopy of methylene blue–smectite suspensions,*** **Journal of Colloid and Interface Science**, 220 (1999) 103-111.

44. H. Lachheb, E. Puzenat, A. Houas, M. Ksibi, E. Elaloui, C. Guillard, J.-M. Herrmann, **Photocatalytic degradation of various types of dyes (Alizarin S, Crocein Orange G, Methyl Red, Congo Red, Methylene Blue) in water by UV-irradiated titania**, Applied Catalysis B: Environmental, 39 (2002) 75-90.

45. D. Rajamanickam, M. Shanthi, ***Photocatalytic degradation of an organic pollutant by zinc oxide–solar process***, **Arabian Journal of Chemistry,** 9 (2016) S1858-S1868.

46. I. Yamamoto, **Nicotine to Nicotinoids: 1962 to 1997, in: Nicotinoid insecticides and the nicotinic acetylcholine receptor**, Springer, 1999, pp. 3-27.

47. L.M. da Costa, T.C. Grella, R.A. Barbosa, O. Malaspina, R.C.F. Nocelli, **Determination of acute lethal doses (LD50 and LC50) of imidacloprid for the native bee Melipona scutellaris Latreille**, 1811 (Hymenoptera: Apidae), Sociobiology, 62 (2015) 578-582.

48. B. Strandberg, L. Strandberg, P.-A. Bergqvist, J. Falandysz, C. Rappe, **Concentrations and biomagnification of 17 chlordane compounds and other organochlorines in harbour porpoise (Phocoena phocoena) and herring from the southern Baltic Sea**, Chemosphere, 37 (1998) 2513-2523.

49. M. Oi, T***ime-dependent sorption of imidacloprid in two different soils,*** **Journal of agricultural and food chemistry**, 47 (1999) 327-332.

50. S. Rakshit, D. Sarkar, P. Punamiya, R. Datta, **Antimony sorption at gibbsite–water interface,** Chemosphere, 84 (2011) 480-483.

51. U. Černigoj, U.L. Štangar, P. Trebše, **Degradation of neonicotinoid insecticides by different advanced oxidation processes and studying the effect of ozone on TiO2 photocatalysis**, Applied Catalysis B: Environmental, 75 (2007) 229-238.

52. M.T.V.S. Savitri, **IMPACT OF SELECTED CHEMICAL PESTICIDES ON MANGO PLANTATION ECOLOGY A CASE STUDY OF RATNAGIRI DISTRICT**, MAHARASHTRA, in, University of Mumbai, 2018.

53. D. Kanakaraju, S. Ravichandar, Y.C. Lim, ***Combined effects of adsorption and photocatalysis by hybrid TiO2/ZnO-calcium alginate beads for the removal of copper***, **Journal of Environmental Sciences**, 55 (2017) 214-223.

54. Z. He, L. Lin, S. Song, M. Xia, L. Xu, H. Ying, J. Chen, **Mineralization of CI Reactive Blue 19 by ozonation combined with sonolysis: Performance optimization and degradation mechanism**, Separation and purification technology, 62 (2008) 376-381.

55. A. Chen, G. Zeng, G. Chen, X. Hu, M. Yan, S. Guan, C. Shang, L. Lu, Z. Zou, G. Xie, ***Novel thiourea-modified magnetic ion-imprinted chitosan/TiO2 composite for simultaneous removal of cadmium and 2, 4-dichlorophenol,*** **Chemical Engineering Journal**, 191 (2012) 85-94.

56. A. Schippers, P.-G. Jozsa, W. Sand, **Sulfur chemistry in bacterial leaching of pyrite**, Applied and Environmental Microbiology, 62 (1996) 3424-3431.

57. S. Wang, Z. Zhu, A. Coomes, F. Haghseresht, G. Lu, ***The physical and surface chemical characteristics of activated carbons and the adsorption of methylene blue from wastewater***, **Journal of Colloid and Interface Science**, 284 (2005) 440-446.

58. D.W. Bahnemann, C. Kormann, M.R. Hoffmann, ***Preparation and characterization of quantum size zinc oxide: a detailed spectroscopic study***, **Journal of physical chemistry**, 91 (1987) 3789-3798.

59. M.T. Yagub, T.K. Sen, H. Ang, E**quilibrium, kinetics, and thermodynamics of methylene blue adsorption by pine tree leaves, Water,** Air, & Soil Pollution, 223 (2012) 5267-5282.

60. T.B.Q. Zorba, **Photocatalytic Degradation of 2-Chlorophenol in Water with Direct Solar Light using Pristine and Kaolinite Supported ZnO**, in, 2015.

61. M.R. Arefi, S. Rezaei-Zarchi, ***Synthesis of zinc oxide nanoparticles and their effect on the compressive strength and setting time of self-compacted concrete paste as cementitious composites***, **International journal of molecular sciences**, 13 (2012) 4340-4350.

62. I. Fatimah, S. Wang, D. Wulandari, **ZnO/montmorillonite for photocatalytic and photochemical degradation of methylene blue**, Applied Clay Science, 53 (2011) 553-560.

63. Z. Yang, Z. Ye, Z. Xu, **Effect of the morphology on the optical properties of ZnO nanostructures,** Physica E: Low-Dimensional Systems and Nanostructures, 42 (2009) 116-119.

64. N. Chandıa, B. Matsuhiro, A. Vásquez, **Alginic acids in Lessonia trabeculata: characterization by formic acid hydrolysis and FT-IR spectroscopy,** Carbohydrate Polymers, 46 (2001) 81-87.

65. P. Laurienzo, M. Malinconico, A. Motta, A. Vicinanza, **Synthesis and characterization of a novel alginate–poly (ethylene glycol) graft copolymer**, Carbohydrate polymers, 62 (2005) 274-282.

66. Y.-Y. Kim, D. Walsh, **Metal sulfide nanoparticles synthesized via enzyme treatment of biopolymer stabilized nanosuspensions**, Nanoscale, 2 (2010) 240-247.

67. M. Jaroniec, ***Incorporation of inorganic nanoparticles into mesoporous carbons synthesized by soft templating***, **The Journal of Physical Chemistry C**, 112 (2008) 11657-11660.

68. A. Leszczyńska, J. Njuguna, K. Pielichowski, J. Banerjee, **Polymer/montmorillonite nanocomposites with improved thermal properties: Part II. Thermal stability of montmorillonite nanocomposites based on different polymeric matrixes**, Thermochimica Acta, 454 (2007) 1-22.

69. M. Nasiruddin Khan, A. Sarwar, **Determination of points of zero charge of natural and treated adsorbents,** Surface Review and Letters, 14 (2007) 461-469.

70. R. Ocampo-Pérez, R. Leyva-Ramos, M. Sanchez-Polo, J. **Rivera-Utrilla, Role of pore volume and surface diffusion in the adsorption of aromatic compounds on activated carbon,** Adsorption, 19 (2013) 945-957.

71. Y. Özdemir, M. Doğan, M. Alkan, **Adsorption of cationic dyes from aqueous solutions by sepiolite,** Microporous and Mesoporous Materials, 96 (2006) 419-427.

72. A. Mills, D. Hazafy, J. Parkinson, T. Tuttle, M.G. Hutchings, **Effect of alkali on methylene blue (CI Basic Blue 9) and other thiazine dyes**, Dyes and Pigments, 88 (2011) 149-155.

73. W.C. Holmes, A.R. Peterson, J.T. Scanlan, **The visual spectrophotometry of dyes**, US Dept. of Agriculture, 1932.

74. Q. Zhou, W. Gong, Y. Li, S. Chen, D. Yang, C. Bai, X. Liu, N. Xu, **Biosorption of Methylene Blue onto spent corncob substrate: kinetics, equilibrium and thermodynamic studies,** Water Science and Technology, 63 (2011) 2775-2780.

75. H.S. Hilal, G.Y. Al-Nour, A. Zyoud, M.H. Helal, I. Saadeddin, **Pristine and supported ZnO-based catalysts for phenazopyridine degradation with direct solar light,** Solid State Sciences, 12 (2010) 578-586.

76. A. Houas, H. Lachheb, M. Ksibi, E. Elaloui, C. Guillard, J.-M. Herrmann, **Photocatalytic degradation pathway of methylene blue in water,** Applied Catalysis B: Environmental, 31 (2001) 145-157.

77. T. Ding, D. Jacobs, B.K. Lavine, ***Liquid chromatography-mass spectrometry identification of imidacloprid photolysis products***, **Microchemical Journal,** 99 (2011) 535-541.

78. S.R.R. Asaad, **Clay-supported sensitized nano-ZnO in photocatalytic degradation of aqueous halophenols using direct solar light**, in, An-Najah National University, 2018.

79. سعید, ناصری, محوی, غلامی, جوادی, ه. برجی ,پرستار, ***Photocatalytic reduction of nitrate in aqueous solutions using Ag-doped TiO2/UV process***, **مجله سلامت و محیط زیست**, 5 (2012) 307-318.

80. A. Agüera, E. Almansa, S. Malato, M. Maldonado, A. Fernández-Alba, **Evaluation of photocatalytic degradation of imidacloprid in industrial water by GC-MS and LC-MS**, Analusis, 26 (1998) 245-250.

جامعة النجاح الوطنية

كلية الدراسات العليا

التحطيم الضوئي المحفز لميثيل الازرق والمبيد العشبي اميداكلوبريد المائية باستخدام دقائق اكسيد الزنك النانوية المثبتة على الجينات الكالسيوم

إعداد

أحلام حسين شفيق زيود

إشراف

أ. د. حكمت هلال

د. عاهد زيود

قدمت هذه الأطروحة استكمالاً لمتطلبات الحصول على درجة الماجستير في الكيمياء، بكلية الدراسات العليا، في جامعة النجاح الوطنية، نابلس – فلسطين.

2021

التحطيم الضوئي المحفز لميثيل الازرق والمبيد العشبي اميداكلوبريد المائية باستخدام دقائق اكسيد الزنك النانوية المثبتة على الجينات الكالسيوم

إعداد

أحلام حسين شفيق زيود

إشراف

أ. د. حكمت هلال

د. عاهد زيود

الملخص

تم استخدام جسيمات ZnO النانوية على نطاق واسع كأشباه موصلات لمعالجة المياه من الملوثات العضوية. استخدم هذا العمل ZnO التجاري والجسيمات النانوية المدعومة لدراسة الامتصاص والتحلل الضوئي للملوثات العضوية المائية. تمت دراسة الميثيلين الأزرق MB (صبغة) وإيميداكلوبريد والذي يستخدم بكثرة في قطاع الزراعة في فلسطين (مبيد حشري)، كملوثات عضوية للمياه. تم تحويل Na-Alginate إلى شكل Ca-Alginate غير القابل للذوبان واستخدامه كركيزة لدعم جزيئات ZnO النانوية. تم فحص النظام الجديد المدعم (ZnO @ Ca-Alginate) بعدة طرق، مثل FT-IR وUV-Visible وTGA وSEM وEDX وXRD. أكدت جميع نتائج التوصيف تكوين ZnO في نظام الحفاز المركب، والذي تم استخدامه في دراسة التحلل الضوئي للملوثات تحت إشعاعات الضوء المحاكاة بالطاقة الشمسية. تم استخدام الكروماتوجرافيا السائلة عالية الأداء HPLC ومقياس الطيف الضوئي UV-visلتحديد الملوثات المتبقية. أظهرت النتائج أن التحلل الضوئي لـ(40 MB جزء في المليون) بواسطة ZnO @ Ca-Alginate وصل إلى خسارة 100٪، بينما وصل(20 imidacloprid جزء في المليون) إلى 56٪ خسارة. تلعب قيم الأس الهيدروجيني ونقطة الشحنة الصفرية pHpzc دورًا رئيسيًا في عملية التحلل الضوئي. كان من الممكن أيضًا استعادة وإعادة استخدام المحفز المركب في تفاعلات تحفيز ضوئي جديدة لبروتين الميثيل، واحتفظ المحفز المستعاد بكفاءته التي قاربت 98 ٪ من التحلل الضوئي لـ MB. كما تمت دراسة العوامل التي تؤثر على عملية التحلل مثل تركيز المادة الملوثة وتحميل المحفز ووقت التشعيع ودرجة الحموضة وكثافة الإشعاع.